Earth and Planetary Science Letters 500 (2018) 225–241

Contents lists available at ScienceDirect

Earth and Planetary Science Letters

www.elsevier.com/locate/epsl

The Hypanis Valles delta: The last highstand of a sea on early Mars?

Peter Fawdon [a,*], Sanjeev Gupta [b], Joel M. Davis [c], Nicholas H. Warner [d], Jacob B. Adler [e], Matthew R. Balme [a], James F. Bell III [e], Peter M. Grindrod [c], Elliot Sefton-Nash [f]

[a] School of Physical Sciences, The Open University, Walton Hall, Milton Keynes, MK7 6AA, UK
[b] Department of Earth Sciences and Engineering, Imperial College London, London, SW7 2AZ, UK
[c] Department of Earth Sciences, Natural History Museum, Cromwell Road, Kensington, London, SW7 5BD, UK
[d] Department of Geological Sciences, Integrated Science Center, State University of New York at Geneseo, One College Circle, Geneseo, NY 14454, USA
[e] School of Earth and Space Exploration, Arizona State University, ISTB4 Room 795, 781 Terrace Mall, Tempe, AZ 85287, USA
[f] European Space Research and Technology Centre, Keplerlaan 1, 2201 AZ Noordwijk, Netherlands

ARTICLE INFO

Article history:
Received 20 March 2018
Received in revised form 23 July 2018
Accepted 27 July 2018
Available online 24 August 2018
Editor: A. Yin

Keywords:
Mars
Mars geology
Mars ocean
delta
fluvial

ABSTRACT

One of the most contentious hypotheses in the geological history of Mars is whether the northern lowlands ever contained an oceanic water body. Arguably, the best evidence for an ocean comes from the presence of sedimentary fans around Mars' dichotomy boundary, which separates the northern lowlands from the southern highlands. Here we describe the palaeogeomorphology of the Hypanis Valles sediment fan, the largest sediment fan complex reported on Mars (area >970 km^2). This has an extensive catchment (4.6×10^5 km^2) incorporating Hypanis and Nanedi Valles, that we show was active during the late-Noachian/early-Hesperian period (~3.7 Ga). The fan comprises a series of lobe-shaped sediment bodies, connected by multiple bifurcating flat-topped ridges. We interpret the latter as former fluvial channel belts now preserved in inverted relief. Meter-scale-thick, sub-horizontal layers that are continuous over tens of kilometres are visible in scarps and the inverted channel margins. The inverted channel branches and lobes are observed to occur up to at least 140 km from the outlet of Hypanis Valles and descend ~500 m in elevation. The progressive basinward advance of the channellobe transition records deposition and avulsion at the margin of a retreating standing body of water, assuming the elevation of the northern plains basin floor is stable. We interpret the Hypanis sediment fan to represent an ancient delta as opposed to a fluvial fan system. At its location at the dichotomy boundary, the Hypanis Valles fan system is topographically open to Chryse Planitia – an extensive plain that opens in turn into the larger northern lowlands basin. We conclude that the observed progradation of fan bodies was due to basinward shoreline retreat of an ancient body of water which extended across at least Chryse Planitia. Given the open topography, it is plausible that the Hypanis fan system records the existence, last highstand, and retreat of a large sea in Chryse Planitia and perhaps even an ocean that filled the northern plains of Mars.

1. Introduction

Whether large seas or an ocean, which might have covered up to a third of the planet's surface, ever existed in the northern lowlands of Mars is one of the most important unanswered questions in the geological evolution of Mars. Evidence to support the ocean hypothesis has come from observations of hypothesised shoreline features in orbital images (Clifford and Parker, 2001; Parker et al., 1993), valley networks terminating at or near these shorelines (e.g., Hynek et al., 2010), and the occurrence of putative deltaic deposits at similar elevations around the dichotomy boundary (Di Achille and Hynek, 2010). Moreover, Gamma Ray Spectrometer observations (e.g., Boynton et al., 2002) suggest excess ice in the subsurface and an enrichment of the D:H ratio indicates a substantial loss of water to space (Villanueva et al., 2015). More recently, the presence of large boulders and lobe-shaped deposits have been explained as tsunami deposits caused by impacts into a martian ocean (Costard et al., 2017; Rodriguez et al., 2016). Nevertheless, identifying consistent evidence of a past standing body or bodies of water (Clifford and Parker, 2001) at a specific time or location in the northern lowlands has proved challenging (Carr and Head, 2003). Moreover it has been argued that there was not enough water to have formed a Noachian-age ocean (Carr and Head, 2015), and a colder, drier ancient Mars is implied instead (Wordsworth et al., 2015). Though this interpretation is contentious, abundant ge-

* Corresponding author.
E-mail address: peter.fawdon@open.ac.uk (P. Fawdon).

https://doi.org/10.1016/j.epsl.2018.07.040

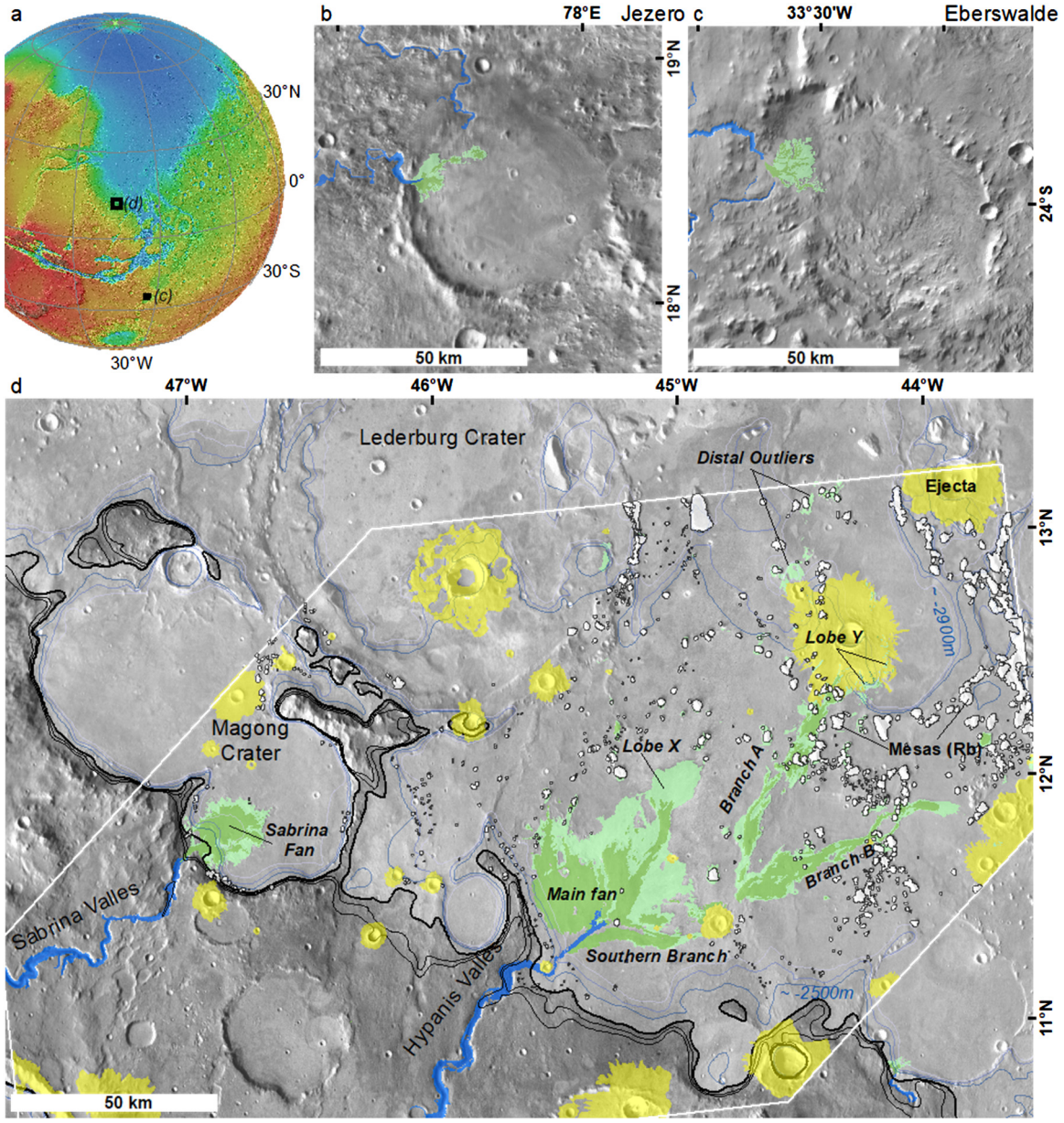

Fig. 1. (a) The location of the Hypanis Valles terminal sediment fan on Mars. Comparison between (b) Jezero (Schon et al., 2012) and (c) Eberswalde (Moore et al., 2003; Rice et al., 2013) deltas. Feeder channels are shown in blue. (d) The extent of the Hypanis and Sabrina sediment fan systems as mapped in CTX data. Here, the 'upper' and 'lower' stratal units are distinguished: Upper fan unit (Ufu), dark green; Lower fan unit (Lfu), light green. Also shown are the rounded buttes (white), impact ejecta (yellow) within the study area (white outline) along with selected MOLA topographic contours at 25 m vertical separation around −2450 m (black), and around −2500 m and −2900 m in blue. A full CTX mosaic can be found as Supplementary material. (For interpretation of the colours in the figure(s), the reader is referred to the web version of this article.)

ological evidence supports a warm and semi-arid climate (Ramirez and Craddock, 2018), however the evidence is incomplete and demands further observations.

Without being able to reliably identify fine-grained oceanic deposits or clear shorelines associated with a large open body of water, alternative evidence for standing water is required. One such piece of evidence could be the presence of sediment fans deposited where a river enters a standing body of water: i.e., delta landforms. Deltaic sedimentary bodies have been identified on Mars but usually occur where river systems enter a crater, forming a confined lake. Excellent examples have been described in Eberswalde, Terby and Jezero craters (Ansan et al., 2011; Bhattacharya et al., 2005; Goudge et al., 2017; Rice et al., 2013; Fig. 1; Wilson et al., 2007). Moreover, an *in situ* example has been described in Gale crater using observations acquired by the Curiosity rover (Grotzinger et al., 2015). Sedimentary fans have been identified around the martian crustal dichotomy along an approximate equipotential surface (Di Achille and Hynek, 2010) and interpreted as deltas, although individually these sedimentary bodies do not necessarily show convincing evidence for a deltaic origin (Kraal et al., 2008; Moore et al., 2003). Recent analysis of stratigraphy in the equatorial Aeolis Dorsa region on Mars has identified possible deltaic deposits and base-level controlled incised valleys suggesting that this region may have formed a palaeo-coastal landscape (Cardenas et al., 2018; DiBiase et al., 2013). However, to establish the possible existence of a northern hemisphere-spanning ocean, evidence is required for the regional development of deltaic sediment bodies (Barker and Bhattacharya, 2018).

Here, we describe the depositional morphology and stratigraphy of a prominent sediment fan body that is located at the

terminus of Hypanis Valles in northern Xanthe Terra (Fig. 1), a Noachian-aged surface (Tanaka et al., 2014) adjacent to the dichotomy boundary (Hauber et al., 2009; Sefton-Nash et al., 2015). The fan is one of many regional sedimentary fans, interpreted to be deltas and alluvial fans (Di Achille and Hynek, 2010; Hauber et al., 2009), found throughout the Xanthe Terra region, but this example is both larger and more complex than other fan-like depositional features in the region, which are generally associated with closed impact crater basins. We focus on detailed planform observations of sedimentary architecture in orbital imagery and digital elevation models. Regional stratigraphy, thermal properties and further hypotheses for the fan's formation are explored by Adler et al. (2018). We show that a parsimonious explanation for key morphologic characteristics of the sediment fan is through deposition as a series of deltaic sedimentary lobes in a standing body of water, as opposed to deposition in a fluvial fan setting (Gupta, 1997). We argue that the fan likely represents an ancient exhumed, and now inverted, delta deposit, and consider the implications of this interpretation for the existence of a large standing body of water in the Chryse basin in the late Noachian or early Hesperian.

2. Methods

2.1. Sediment fan and drainage network mapping

We used Context Camera (CTX; ~6 m/pixel, Malin et al., 2007), High Resolution Imaging Science Experiment (HiRISE; ~25 cm/pixel; McEwen et al., 2007) images and THermal EMission Imaging System data (THEMIS; Christensen et al., 2004) to investigate the morphology, sedimentary architecture, and depositional environment of the Hypanis sediment fan complex and catchment region.

Observations and measurements were made using ArcMap and ArcScene Software. Basic geological mapping units were delineated in CTX data based on their texture at the scale of CTX data (~1:10,000) supported by observations from THEMIS and HiRISE (see supplementary material for details). For three-dimensional analysis, we created digital elevation models from both CTX and HiRISE stereo observations in Integrated Software for Imaging Spectrometers (ISIS) and 'SocetSet' software following the methodology of Kirk et al. (2008). The post spacing of the DEMs were ~20 m for CTX and ~1 m for HiRISE. Vertical precision of the DEMs was controlled to Mars Orbital Laser Altimeter (MOLA; Smith et al., 2001) data. A CTX DEM Mosaic was made by geo-referencing the orthrorectifed image cube and blending along a radiance seamline.

To estimate the potential area of the catchment (Fig. 2), a Hypanis Valles drainage network map was calculated using the ArcMap 10.4 Spatial Analyst 'ArcHydro' toolset (Esri, 2016) to determine the watershed area and to relate the network morphology and timing to the fan lobes. Flow direction and accumulation grids were created using the MOLA DEM. Errors in the DEM that created sinks or basins were filled prior to calculating direction and accumulation. This drainage network was then compared to a manually created river network, mapped on a CTX mosaic for quality control. The ArcHydro-derived drainage network deviated significantly from the mapped network in regions where impact craters post-date flow and was therefore manually edited to remove erroneously generated channel segments that filled or stretched across these basins. The head regions of the southern Hypanis branch, and the medial and distal reaches, compare well in both methods. The overall drainage network area and stream ordering were determined from the edited ArcHydro product.

2.2. Crater count methods

The timing of deposition of the Hypanis sediment fan is poorly constrained. Current estimates, based on crater counts from the fan surface, places fluvial activity within the Hesperian to Early Amazonian epochs (Hauber et al., 2013), relatively late in Mars' history. However, conventional crater count methods are possibly unreliable, given the small areal extent of the deposits and due to post-formational resurfacing fan that is evident by the inverted morphology (e.g., Warner et al., 2015). Instead, we utilize two methods to constrain relative age: (1) relative superposition of the Hypanis valley system by a large, 70-km diameter impact crater, and (2) buffered crater counts. The ejecta of a 70-km-diameter unnamed crater, (Fig. 2), was found to fully superpose both the southern and eastern tributary branches. For this crater, all superposing craters >1 km in diameter were counted within a 27 km wide annulus that extends from the crater rim. Within the annulus, the ejecta is thick enough that all 1 km diameter craters are superposing. The counts were compared against the production and chronology functions of Hartmann (2005) and Michael (2013) as well as that of Ivanov et al. (2001).

In the second case, the Cratertools 'buffered crater counting' extension was used to count craters with diameters >500 m that superpose the Hypanis channel network (Kneissl et al., 2015). In the buffered counting method (Fassett and Head, 2008), developed to provide age estimates for linear features, the size of the area buffer is dependent on the diameter of the crater that superposes the channel. A unique buffer is applied to every crater in the count and the crater frequency is calculated for each individual crater separately. We apply both the one radius and three radii buffer methods to determine the count area. The one radius method refers to a buffer size that is 0.5 times the diameter of the counted crater and is intended to include only those craters whose rims superpose the channel. The three radii method generates a buffer that is 1.5 times the diameter of the crater. In this case, all craters whose ejecta blankets superpose the channel are included. The data were then compared to published production and chronology functions.

3. Observations and interpretation

3.1. The Hypanis Valles catchment

The equatorial Xanthe Terra region of Mars exhibits multiple fluvial systems that are incised into late Noachian-age highland terrain and source sedimentary fans, including the Hypanis and Sabrina Valles fans. Hypanis Valles is a bedrock-eroded trunk valley that debouches into Chryse Planitia and forms from three major contributing branches reaching a maximum observable length of ~1000 km (Fig. 2). The valley is narrow (1.5–3 km in width) with a sinuous planform and is incised up to 75 m into the Noachian bedrock. The total watershed area is $\sim 4.6 \times 10^5$ km^2 as determined from the ArcMap catchment model, which includes the watersheds of Hypanis, Nanedi Valles and Drilon Valles. CTX images reveal that the downstream reach of Nanedi continues as a small (~500 m) inner channel, incised into the floor of the southern tributary of Hypanis. This suggests that the large upstream catchment of Nanedi may have sourced water and sediment through Hypanis and out to the Hypanis fan system. This also indicates that Nanedi may be a younger system relative to Hypanis. The combined Hypanis/Nanedi watershed is an order of magnitude larger than the estimated catchments of the sediment fans of Eberswalde crater (Irwin et al., 2015), Jezero crater (Goudge et al., 2015) and Gale crater (Table 1). The elevation data and drainage network map indicates that overland flow of the Hypanis–Nanedi system originated from the highlands that surround Carmichel crater and the region west of Orson Welles crater. There is no obvious genetic connection between the Hypanis–Nanedi network and the nearby Hesperian to early Amazonian-age circum-Chryse outflow channels (Hauber et al., 2009; Nelson and Greeley, 1999).

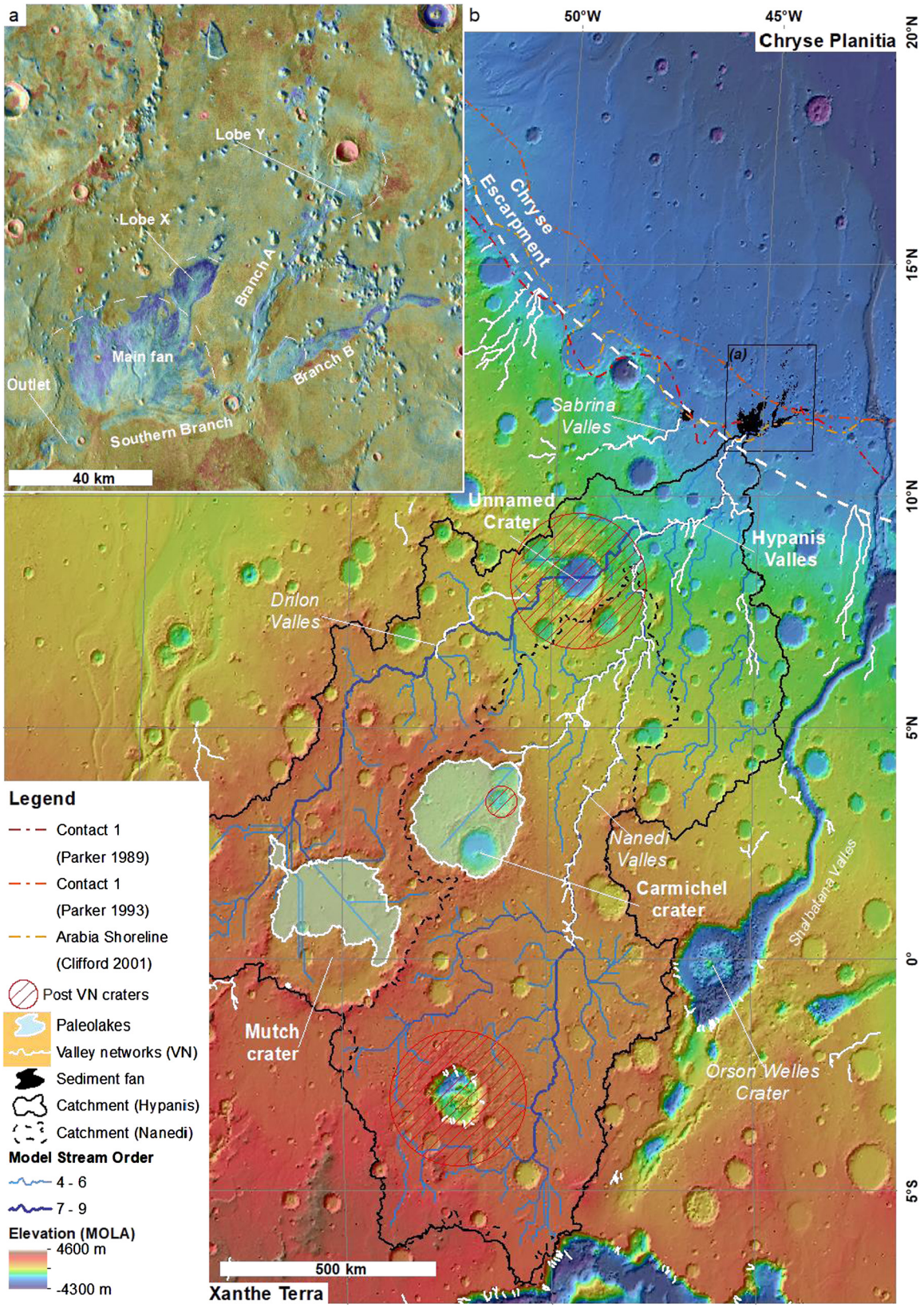

Fig. 2. Hypanis Valles catchment and sediment fan system: (a) THEMIS night-time data showing the sediment fan, branches (A and B), and lobes (X and Y) as low thermal inertial deposits (blue) on the scale of 100 m against the higher thermal inertial Ppu surface (red). The lower thermal inertia suggests the fan's surface is composed of finer or more poorly cemented grains than the surrounding materials. This matches observations of extensive aeolian materials on the fan deposits; (b) Context and model catchment across Xanthe Terra showing: the extent of the Hypanis and Sabrina sediment fans (black); the valley network of Hynek et al. (2010) identified in THEMIS data (white); the hydrological model extent of the catchment for Hypanis (black line) which incorporates the model catchment for Nanedi Valles (dashed line) and the model Strahler stream network (Strahler, 1957; orders 4 to 9; light to dark blue). Also shown are major craters that likely postdate the majority of activity in the valley network (red hash).

Table 1
Comparison of deltas on Mars.

Delta	Fan area (km^2)	Watershed area (km^2)	Basin type	Location
Hypanis	970	46.1×10^4	Open	11°N, 45°W
Jezero[a]	65	3.1×10^4	Open (Jezero crater, drains to Isidis Planitia)	18°N, 77°E
Eberswalde[b]	125	1.7×10^4	Closed (Eberswalde crater)	24°S, 33°W
Sabrina[c]	256	–	Unclear (Magong crater)	12°N, 47°W
Terby[d]		–	Open (to Hellas Planitia)	28°S, 74°E

[a] Goudge et al. (2015).
[b] Irwin et al. (2015).
[c] Platz et al. (2014), Knade et al. (2017), Hauber et al. (2013) & Fig. 1.
[d] Ansan et al. (2011).

3.2. The Hypanis sediment fan

The Hypanis sediment fan is a ~40 km wide and ~60 km long inverted sedimentary deposit located north of the regional break in slope that demarcates the boundary between the Noachian-age Xanthe Terra region, Hesperian aged transitional units and the Amazonian-age surface of Chryse Planitia (Tanaka et al., 2014, Fig. 2b). This sharp regional transition, termed the Chryse escarpment, is characterised by a change from terrain hosting numerous heavily degraded impact craters upslope of the escarpment (rims and ejecta removed, floors infilled during the Noachian (Craddock et al., 1997; Irwin et al., 2013), to the topographically smoother plains downslope, which host numerous infilled 'ghost' craters and craters with lobate continuous ejecta margins (Barlow et al., 2000; Salvatore and Christensen, 2014). The transition in bedrock geology occurs at the same elevation as the Hypanis and Sabrina outlets which suggests that the transition to deposition north of the Chryse escarpment was partly topographically controlled.

The Hypanis fan is clearly distinguished using THEMIS nighttime surface temperature data, in which the sedimentary fan body shows a dark tone implying a low thermal inertia relative to the surrounding mid-toned plains and brighter terrains surrounding the fan (Fig. 2a). We sub-divided the fan and associated deposits into three map units: the fan is comprised of the Upper and Lower fan units (Ufu and Lfu; Fig. 1d), whilst the bedrock geology of the surrounding plains is mapped as the Peripheral plains unit (Ppu; Fig. 1d). The main sediment fan (Ufu and Lfu) forms an approximately semi-circular arcuate body, with several flat-topped ridges branching off and extending 140 km to the north-east (Fig. 1d). The elevation of these deposits descends 500 m from −2475 m at the Hypanis Valles outlet to ~ −3000 m for the most northerly mapped outcrops (Fig. 1d). The Peripheral plains unit (Ppu) consists of dark toned low relief material with numerous darker smooth patches that extend away from the margins of the sediment fan. The unit appears to retain small (<0.5 km) craters however these have degraded or no rims and often have layers of material inside them (Fig. 4d). Where the unit approaches the main fan it has a smoother texture exhibiting polygonal fracture patterns (Fig. 5b). Outliers of Ppu material occur on top of the strata of the main fan (Figs. 3b, 5a) and on a HiRISE scale this unit is clearly stratigraphically interbedded with the margins of the sediment fan (Fig. 4c). Traced westwards, this material onlaps the degraded outer rim of Magong crater, approximately following the −2500 m MOLA contour. To the east, a cluster of rounded buttes appear to overlie the unit. The present day surface eroded into the Ppu slopes to the north, and is topographically open to Chryse Planitia and are overlain by material of the early Hesperian transition unit (eHt) in the global stratigraphy of Tanaka et al. (2014).

3.3. Proximal Hypanis sediment fan body

The proximal Hypanis sediment fan deposit covers an area of ~970 km^2 and forms an irregular 25 km-radius semi-circular arc that radiates from the outlet of Hypanis Valles (Fig. 3a). Analysis of the fan in CTX and HiRISE data show that the fan body is comprised of several complex interlayered sedimentary deposits (Figs. 3b, 4).

Numerous observations of layering and steep scarps suggest that most, perhaps all, of the fan body is formed of competent sedimentary rock. The Upper and Lower fan units (Ufu and Lfu), are characterised by different surface textures and exhumation levels (Fig. 1d). The Upper fan unit outcrops in the southern part of the fan, the upper surface of which occurs at a higher elevation than the Lower fan unit. This upper exhumed surface of the Ufu unit (dark blue, Fig. 1d) shows a dense network of crosscutting, straight to curving lineations that sometimes form low relief ridges (Figs. 3c, 4a). In the western part of the proximal fan, the lineations are orientated approximately N-S (Figs. 3a, 4a). In contrast, in the eastern part of the fan, the lineations are orientated E-W. The lineations locally appear to define elongate 10–100 m-wide 'corridors' that cross-cut one another (Fig. 4a). The internal stratigraphy of the Upper fan unit is exposed along an erosional scarp that defines its northern mapped extent. This ~20–30 m high scarp exposes contiguous, meter-scale, sub-horizontal layering that confirm the presence of stratification within the fan (Figs. 3b, 4a).

The Lower fan unit has a mapped surface area of ~250 km^2 and is exposed to the north of the Upper fan unit. The upper surface of this stratal unit shows abundant NW-SE-trending ripple-like features known as Transverse Aeolian Ridges (TARs; e.g., Balme et al., 2008; Fig. 3b). However, gaps in TAR coverage show that the Lfu is comprised of light toned, smooth-textured sedimentary material with occasional low-relief mesas and polygonal fractures that often occur in shallow flat-bottomed pits (Figs. 4a, 5b).

Extending 100 km north from main sediment body is the widespread Peripheral plains unit (Ppu). This unit has a variety of surface textures and has a complex relationship with the Hypanis sediment bodies and the adjacent highlands. The Upper fan unit generally occurs at a higher elevation than the Ppu and is often separated from the Ppu by an erosional scarp and Lfu, except south of the main fan, and in a depression on the western margin of the main fan (Figs. 6a and 4d). The Lower fan unit (Lfu) generally overlies the Ppu, though the boundary sometimes appears gradational, and the contact is obscured or ambiguous in many places (Figs. 5b, 6c). Adjacent to the sediment fan, the Ppu shows a smooth surface characterised by polygonal fractures (Figs. 4, 5), but traced further from the sediment fan the surface is rockier and appears to retain numerous small craters. Numerous dark patches, commonly associated with subtle topographic lows are observed (Figs. 6b, 7c).

The Upper and Lower fan units comprise lobate bodies that protrude northwards into the Chryse Planitia basin. The northern margin of the Upper fan unit is highly irregular forming distinct finger-like projections (Fig. 3a), which suggests that these may rep-

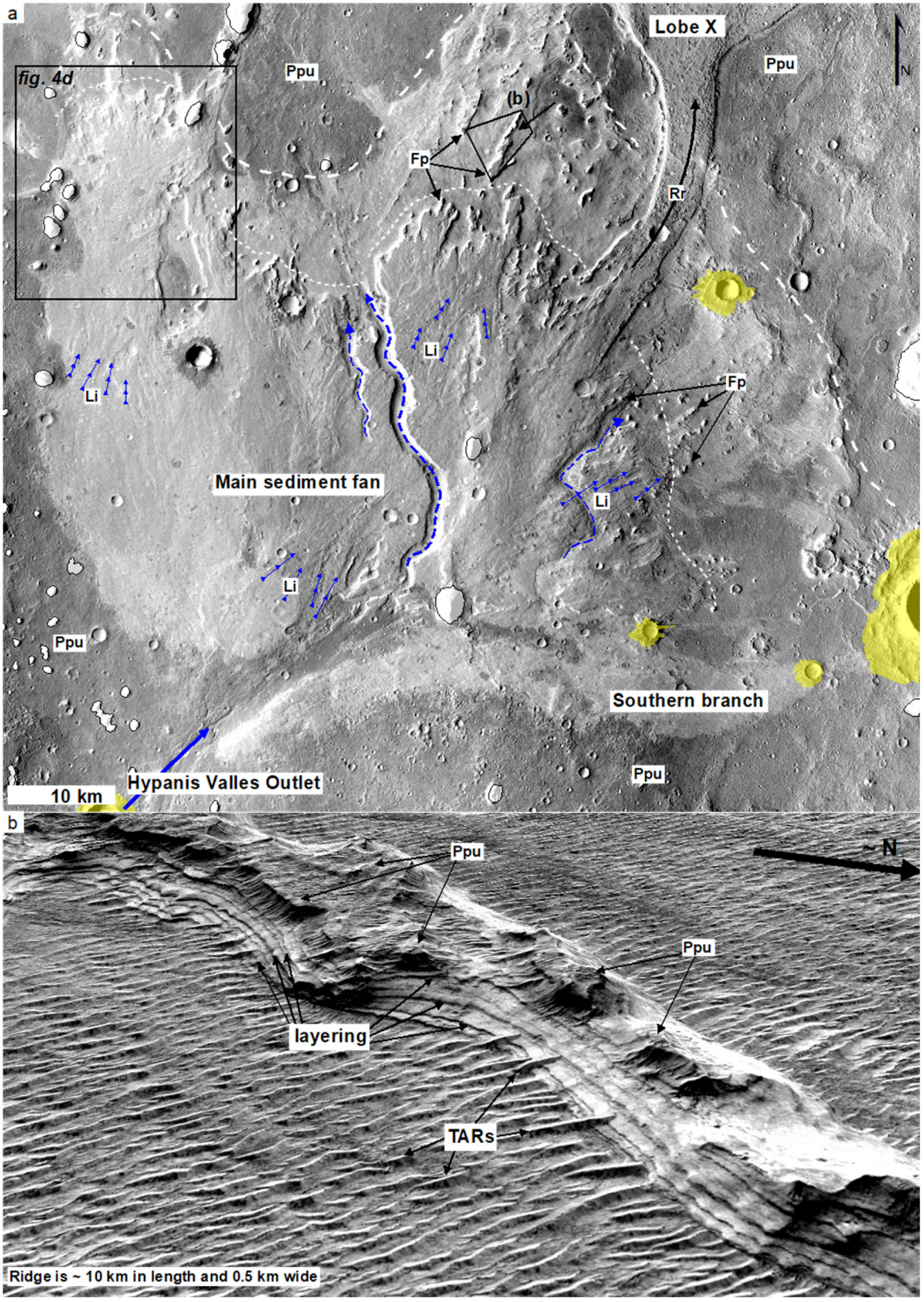

Fig. 3. (a) The proximal sediment fan at the termination of Hypanis Valles showing: The direction from the outlet (blue line); the irregular erosional scarp between the upper (Ufu) and lower (Lfu) fan surfaces (dotted line); gradational boundary between the Lfu and Peripheral plains material (Ppu; dashed line); low-relief 'braided/lattice' lineations on the upper surface of the main fan (Li); ribbon-like ridges showing basinward routing of sediment (Rr); late-stage incised channels (dashed blue arrows); rounded buttes of remnant overburden (white unit); Peripheral plains material (Ppu). (b) A finger-like projection from the main fan showing layers which can be traced for tens of kms and outliers of Ppu on top of the ridge. NW-SE trending TARs can also be seen.

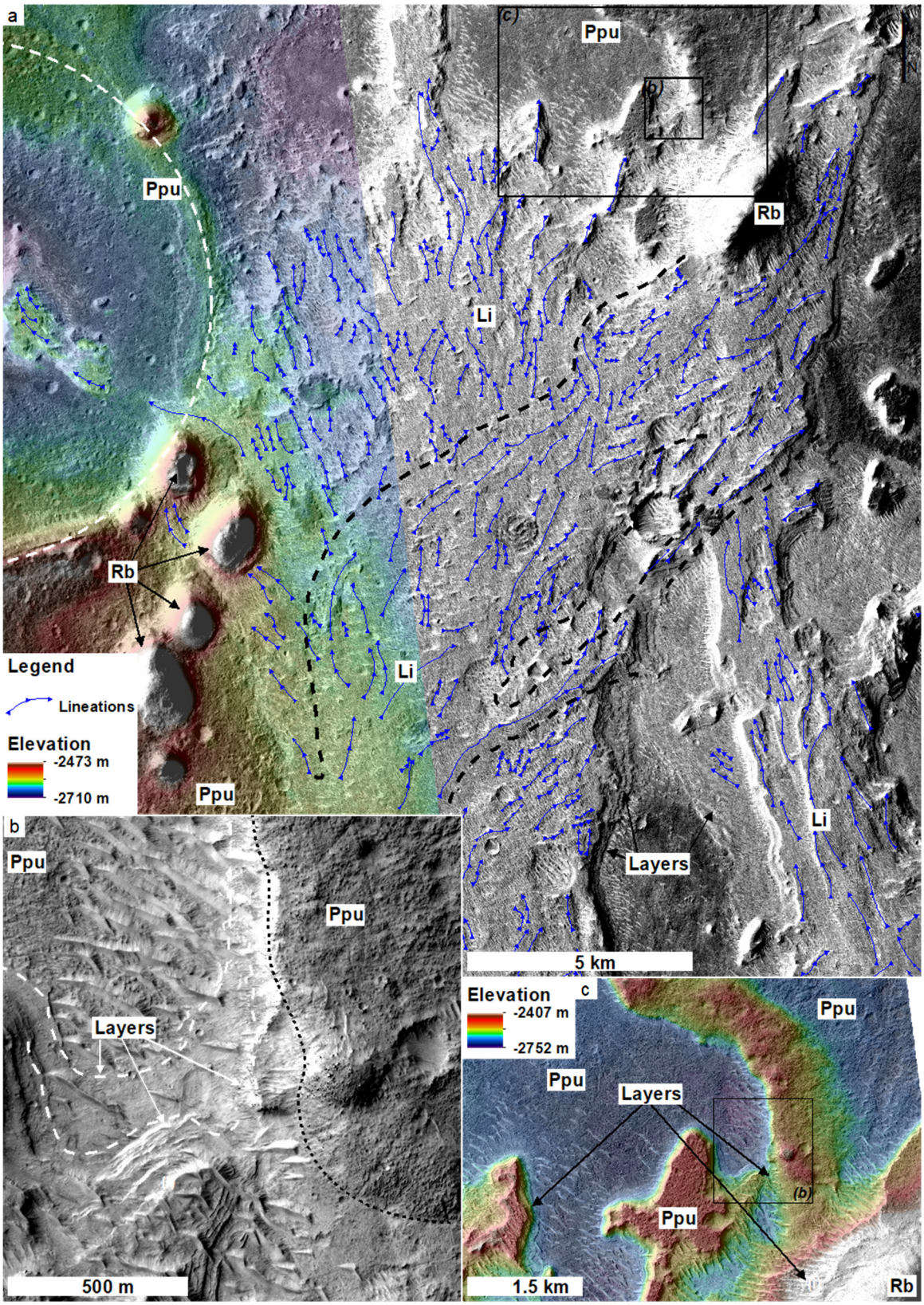

Fig. 4. (a) The layering and stratigraphic relationships of the main fan, showing interlaced straight to curving, 10–100 m wide, low relief ridges (Li; blue arrowed lines). Examples of layering exposed in the 20–30 m high scarp at the transition between the Upper and Lower fan unit which transitions into the polygonally fractured parts of the Ppu. Also seen are examples of the Ppu overlying distal parts of the fan and a ghost crater (dashed line) that is infilled by a spur of fan material from the main fan. Both the fan and plains unit are overlain by the rounded buttes (Rb). These relationships are also shown in (b) and (c) topographic data HiRISE image ESP_037651_1920 (DTM 7, see supplementary information) where elements of the fan material (both sub-figures, layers: white dashes) are overlain by, and overlie, material associated with the Ppu (both sub-figures, boundary: black dotted line). Both units underlie the rounded buttes (Rb).

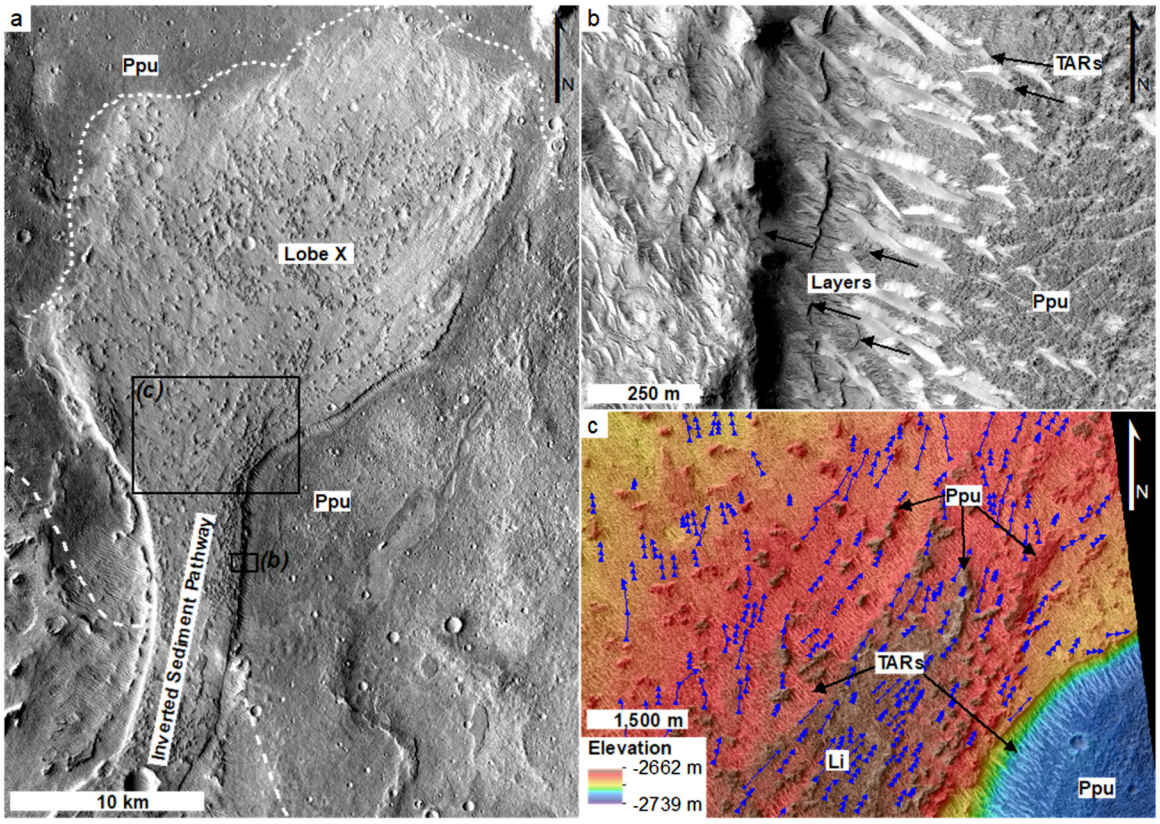

Fig. 5. (a) Lobe X: the inverted sediment pathway and Lobe X overstepping the extent of the Upper and Lower fan stratal units (dashed lines). Subtle lineations are visible on the upper surface of this lobe. (b) Detail from the inverted sediment pathway in HiRISE ESP_034394_1920 showing the dark fractured Ppu, layers within the ridge and TARs associated with the fan units. (c) The surface of Lobe X showing lineations on the surface (Li) and dark outliers of Ppu material overlying Lobe X in HiRISE ESP_034394_1920 DEM 9 (see supplementary information).

resent an erosional remnant of formerly more extensive deposits that have been eroded by southward scarp retreat, exposing underlying strata of the Lower fan unit during this process. Kilometre scale hills and buttes occur across the northern outcrops of the sediment body and across the surrounding plains (Figs. 2, 3a, 4). Close examination of these features indicates that they superpose the fan deposits, rather than protruding through from beneath them. They are therefore likely erosional remnants of an older, and previously more extensive, overburden deposit that once superposed the sediment fan and the wider area.

We interpret the lineations and ridges of the Upper fan unit (Fig. 3) as the intersection of multiple channel accretion deposits with the present-day surface. Interestingly, we do not observe any sinuous channel forms. The ridges appear braided or crosscutting on a length scale of tens of meters and terminate in small subsemicircular fan-like arrangements (Fig. 3c). A clear example of the relationship between the Upper fan unit and the underlying topography is observed on the western margin where fan superpose what is now a ghost crater (Fig. 4a), thereby demonstrating the presence of an unconformity between underlying materials and fan deposits.

3.4. Channel-lobe body X

Channel-lobe body X (Figs. 1, 5) comprises a ribbon-form sediment body (Cuevas Martínez et al., 2010; Gibling and Rust, 1990), a narrow, elongate sediment body with a sub-sinuous planform, that has a lobe-shaped sedimentary body at its terminus. The ribbon-body initiates within proximal fan strata and then extends northward beyond its northern margin. North of the Hypanis Valles outlet, it forms a ∼2 km wide and ∼13 km long flat-topped ribbon-form body. The margins this feature shows that it is comprised internally of 1–5 m thick layers in HiRISE images suggesting a sedimentary origin (Fig. 5b). Beyond the proximal fan deposits, this feature forms a ∼50-m-tall ridge in the current landscape (Figs. 2b, 3a, 5). Here the ribbon-form body shows steep, cliff-forming margins and overlies the Peripheral plains unit. At the contact with the Peripheral plains unit, a gradational transition from the layered ridge to smooth fractured material is observed, which shows transition into more rugged, but still fractured, surfaces (Fig. 5b, c).

Approximately 50 km north of the Hypanis Valles outlet the ribbon body expands to form a lobate sedimentary rock body that is ∼10 km wide and 13 km long (Fig. 5). Metre-scale layering is observed in sections at the margins of this body. This lobate body has a convex-up cross-profile and has a maximum thickness of ∼75 m. At its northern margin, it tapers out and shows abrupt transition into the Peripheral plains unit. The nature of this contact is unclear in orbital images. The upper surface of the lobate body is covered in abundant TARs, but straight to slightly curving lineations (Figs. 3, 5a) can be observed through the loose cover associated with TARs (Fig. 5a). These lineations appear to radiate away from the apex of the ribbon-like ridge that connects to it Lobe X to the main fan.

We interpret the ribbon-lobe sediment body to form a single connected sediment routing system derived from the Hypanis outlet. The ribbon body is interpreted as the now inverted form of a fluvial channel belt (Cuevas Martínez et al., 2010). In its southern reach, the channel deposits are elevated by ∼25 m above the distal parts of the proximal fan deposits in the HiRISE DTM (see supplementary material), indicating that they stratigraphically overlie, and are therefore younger than, the most of the proximal fan. Northward beyond the fan, the channel steps out across plains material indicating that it oversteps the edge of the fan.

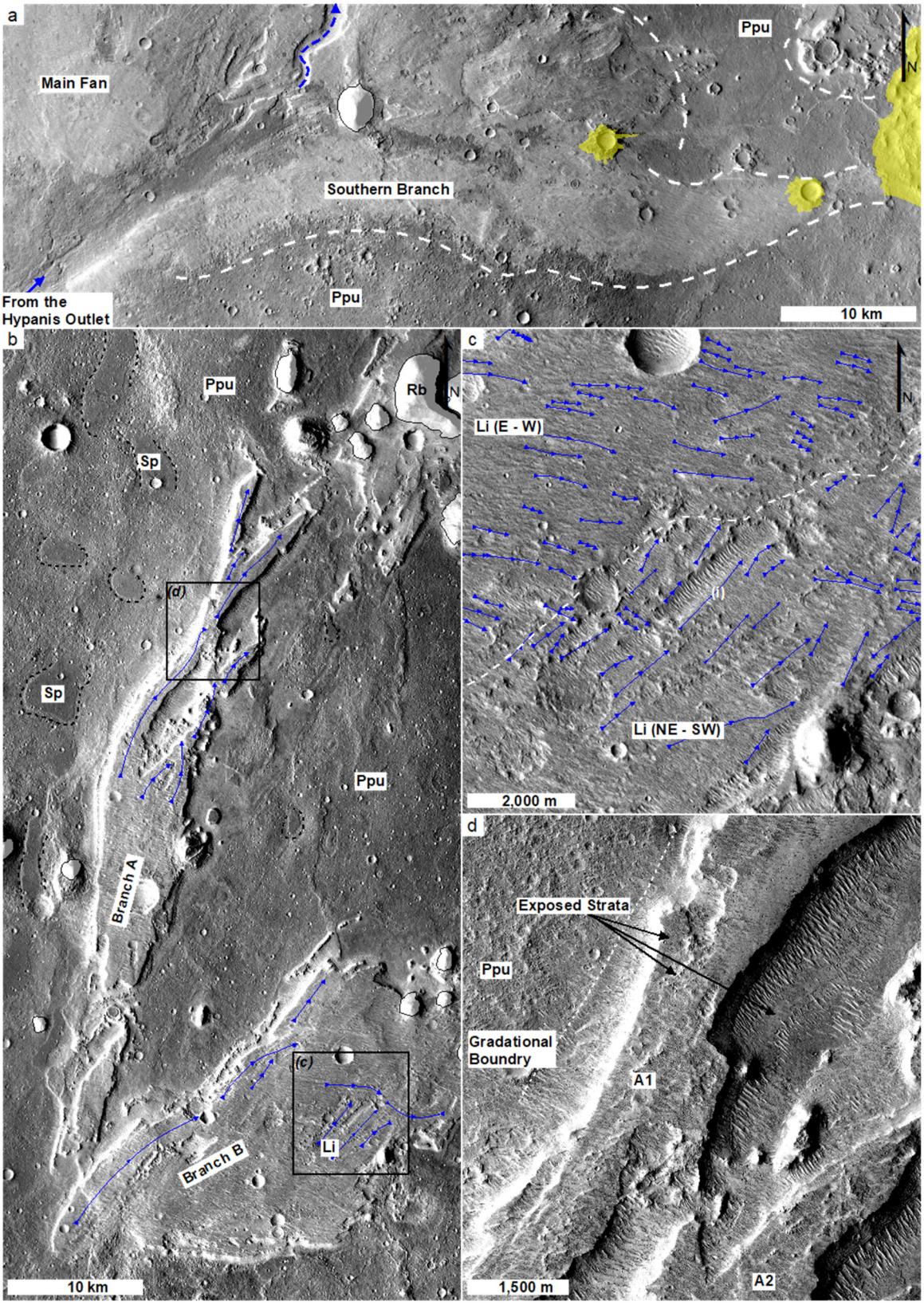

Fig. 6. Branches of the Hypanis sediment fan system. (a) The Southern Branch sediment body shown in association with Peripheral plains (Ppu) and the Hypanis outlet (blue arrow), which is associated with late-stage erosional channels (blue dashed arrow) cutting though the sediment fan. The Southern Branch is overlain by rounded buttes (Rb) and impact ejecta to the east. (b) Branch A is formed of curvilinear, interlaced branching inverted channel segments, overlain by rounded buttes (Rb) to the north and surrounded by Ppu with smooth patches (Sp). Branch B shows a sediment body with low relief ridges exposed (Li). In detail (c) this sediment body shows several strata including a surface with W-E lineations (Li, blue arrowed lines) in HiRISE PSP_010817_1920 DEM 10 (see supplementary material) and a subjacent surface with low relief lineations (Li) trending NE. Again, layering is seen in the steep ridge flanks. (d) The surface of ridge A shows a complex twin-ridge system (Ridge A1 and A2) that suggests it is made of several different stratal units. Ridge A shows a gradational boundary with the Peripheral plains unit (Ppu).

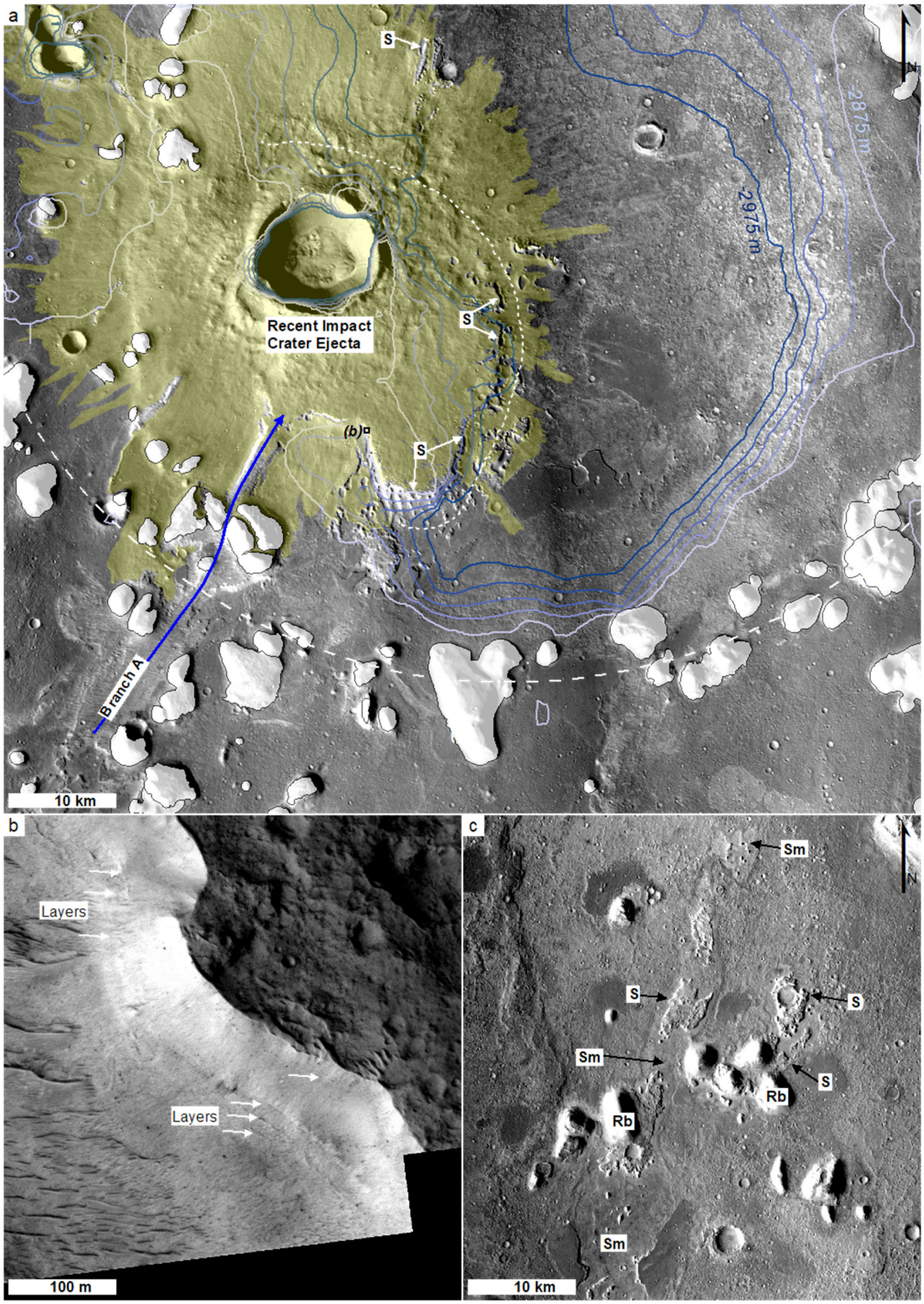

Fig. 7. (a) A sediment fan in a local topographic low, likely 'ghost crater' at ∼−2900 m shows (i) the end of Branch A, crossing the rim of the ghost crater (white long-dashed line) terminating in sediment fan Lobe Y (approximate margins shown by short dashes). The edges of the sediment fan crop out from the mantling of impact ejecta (S). The sediment fan occurs in a topographic low, contours are shown descending from −2875 m (lightest blue) to −2975 m (darkest blue), circumscribed at the rim of the ghost crater by rounded buttes (Rb). (b) Some layering is seen in the edge of the fan where it exposed. However, this area is significantly less eroded than the main fan and is mantled by impact ejecta so appears more massive. (c) Flat topped bright ridge segments underlying rounded buttes (Rb). The ridge segments appear to be distal remnants of inverted channels set in smooth parts (Sm) of the Peripheral plains (Ppu).

The lobate body is a distinct feature formed by deposition of sediment at the terminus of a feeder channel that has itself become sediment-infilled. The presence of linear features radiating from the apex of the ribbon body suggest that these are bedset boundaries expressed on the upper erosional surface of the lobate body. We interpret these lineations to have formed by infill of laterally shifting, elongate distributary channels that coalesced to form the lobate body. The observation that the lineations appear to radiate from the transition from the ribbon channel to the lobe (Fig. 5c) suggests that this apex forms a channel furcation node; channels emerging from this apex avulsed around this node building the lobe shaped feature.

3.5. Inverted channel branches

Extending from the Hypanis Valles entry point (Fig. 6b) and the eastern margin of the proximal fan, are a series of branching ∼1 km wide flat-topped, ribbon-form sediment bodies (branches A and B). These have a similar thermal inertia (low on the scale of 100's m) to the proximal fan material (Fig. 2b). CTX and HiRISE data show that outcrops of these ridges extend discontinuously up to 170 km northeast from the Hypanis Valles outlet. The longest continuous ridge sections comprise two clear branches, A and B (Fig. 1). These appear to be connected to the Hypanis Valles outlet via an east-west oriented, elongate sediment deposit that lies at the south-eastern boundary of the proximal fan and the southern highlands terrain (Figs. 1, 3a, 6a). This "Southern Branch" clearly connects with the northeast trending Branch A and east trending Branch B (Fig. 1), although the detailed relationships are obscured by an impact crater.

Commencing from the edge of the main fan (and the end of the Southern Branch) both branches A and B extend, discontinuously, at least ∼60 km towards the east and northeast. They do not overlie older fan bodies but occupy an area at the eastern margin of the proximal fan deposit and overlie the Ppu. Branch A comprises two slightly sinuous sub-branches that form a discontinuous, occasionally connected, curvilinear path (Fig. 6b). Traced northwards, segments of the discontinuous ridge crop out between a cluster of rounded buttes before passing into Lobe Y (Fig. 2; described in the next section). Branch B initiates as a ∼15 km wide, flat-topped, mesa-forming sediment body (Fig. 6b). Traced eastwards, Branch B narrows, forming a simple, flat-topped, <1 km wide ridge that is slightly sinuous (<1.14), that has an approximately NE-SW-orientation with. The distribution and shape of ridge components (Fig. 6a) in both branches strongly suggests that they represent the eroded remnants of formerly more extensive sedimentary deposits.

The upper surfaces of both branches, although locally covered in TARs, show discontinuous straight to curving lineations similar to those observed on the upper surface of the proximal fan (Fig. 6c, d). These lineations are oriented subparallel to the elongation direction of the branches. Sets or groupings of these lineations appear to cross-cut each other, and locally define elongate ridges. These surface textures occur in different stratigraphic layers (1–5 m thick) that have consistent elevations, but cross-cut one another in places. These linear features are interpreted as bedset boundaries expressed in planview similar to on the proximal fan body and in Lobe X (Fig. 6c). The flanks of both ridges contain meter-scale, sub-horizontal layering that is traceable over tens of km (Fig. 6d). We interpret the ribbon-like forms to be palaeo-fluvial channel belts that aggraded in an alluvial setting and that are now expressed in inverted relief. The elongate inverted ridges are consistent with deposition as ribbon-form fluvial channel belts tens of kilometres in extent in an ancient alluvial/deltaic plain which subsequently became topographically inverted (e.g., Cardenas et al., 2018; Cuevas Martínez et al., 2010). The presence of stratigraphic layering within these ridges, and the occurrence of diverging sets of lineations parallel to the elongation direction of the ridges is consistent with a sedimentary origin. The presence of two distinct ridge systems (Branches A and B) suggests a distributary system with furcation of these systems occurring downstream of the Southern Branch (Fig. 1). The preserved width of the ridges and internal structure is suggestive that the ridges are not former channels but rather channel belts.

3.6. Distal Lobe Y and additional deposits to the north

At the northern termination of Branch A, located ∼100 km northeast of the Hypanis Valles outlet (Fig. 1), the Branch crosses is overlain by a group of buttes at the edge of a local topographic low. Here the ∼1 km wide ridge expands to form a lobate feature that is ∼10 km wide and ∼15–20 km long mostly mantled by impact ejecta (Fig. 7a). This lobate body, whilst largely mantled by impact ejecta is comprised of light-toned material with stratification being observed within its eastern scarp (Fig. 7b). We interpret this body to be a sedimentary rock body. Whilst it is mantled and partially obscured by a relatively fresh impact crater, the transition from a ribbon form ridge into the lobate body is well preserved. A key feature of this deposit is that it is located within the remnant of a 40-km-diameter ghost crater, the rim of which is demarcated by a ring of mesas (Fig. 7a). Branch A inverted channel crosses the rim of the ghost crater before showing expansion to form the lobe deposit, which is set within a topographic depression defined by the crater (Fig. 7a). This suggests that the lobe is a fan deposit located at the end of the sediment pathway now represented by the inverted channel form, and its deposition here may be associated with the palaeotopography of the 40-km-wide impact structure (Fig. 7a).

Forty kilometres to the north of Lobe Y, a discontinuous and degraded series of outcrops representing possible remnants of ribbon-form segments of inverted channels are observed, at a distance ∼170 km from the main Hypanis outlet (Fig. 1). Surface textures on these outcrops are similar to those observed on the ribbon-form sediment bodies to the south, suggesting they likely represent the most northerly and most basinward remnants of the Hypanis depositional system (Fig. 7c). These structures occur at an elevation of ∼−3025 m but are not confined in a northwards direction by any material of the same age or older. This implies that the section of the basin infilled by these sedimentary deposits is, and almost certainly was at time of deposition, topographically open to the northern plains of Mars (Figs. 2, 9). Moreover, this indicates that deposits of the Hypanis sediment routing system occur many tens of kilometres basinwards of the Hypanis outlet suggesting extensive progradation of the system.

3.7. Late-stage erosion of the sediment fan

The preservation of the proximal fan, and the associated branching ribbon-like ridge and distal lobes in inverted relief indicates that the sedimentary succession has experienced post-depositional and post-lithification erosion (DiBiase et al., 2013; Williams et al., 2009). The inversion of relief preservation style (Pain et al., 2007; Pain and Oilier, 1995) occurs where more-resistant materials armour the surface against erosion, while adjacent less-resistant materials are denuded (Burr et al., 2009; Pain et al., 2007; Pain and Oilier, 1995; Williams et al., 2009; Davis et al., 2016). Given the geological setting the channel deposits are probably predominantly cemented sandstones as inferred from the layering, albedo, thermal inertia, association with TARs, and by analogy with similar landforms on Earth (Burr et al., 2009; Cuevas Martínez et al., 2010; Williams et al., 2009; Zaki et al., 2018). Thus, materials deposited in the larger channels

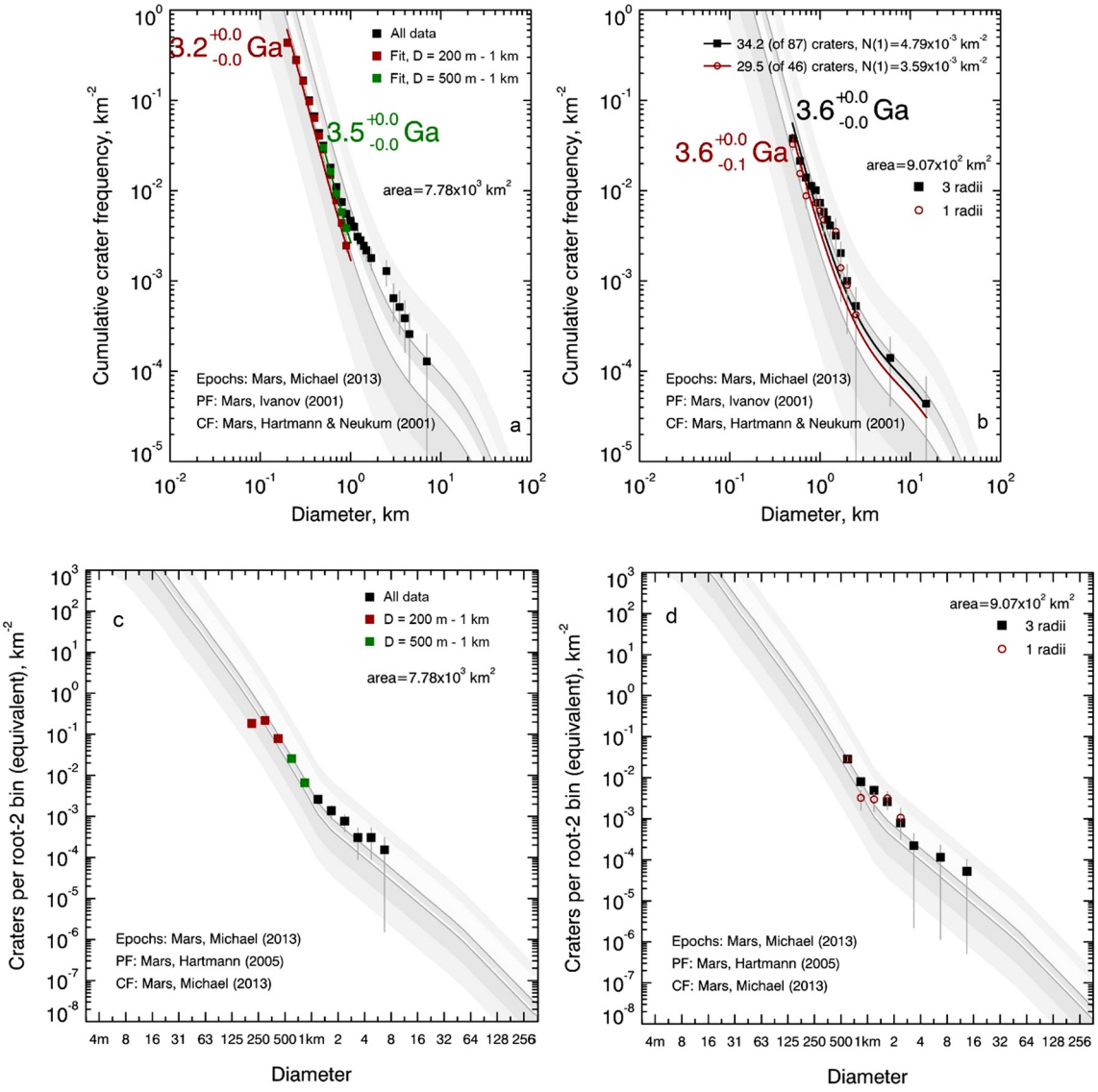

Fig. 8. Impact crater cumulative size frequency distribution plots with fitted model ages for (a) the unnamed crater (Fig. 2b) and (b) Hypanis Valles using the buffered crater counting method of Fassett and Head (2008). The data are consistent with observed superposition relationships that suggest Hypanis Valles is older than the unnamed crater. The N(1) values for both indicate an early Hesperian formation age. N(0.5) values indicate a late Hesperian retention age for the unnamed crater and an early Hesperian age for Hypanis. Root-2 binned incremental size-frequency plots (2005) for (c) the unnamed crater and (d) Hypanis Valles buffered counts. The N(1) and N(0.5) value suggests an early Hesperian crater age for the unnamed crater. N(1) and N(0.5) values for Hypanis Valles suggests an older age of late Noachian and early Hesperian, respectively.

probably protected deposits beneath them, while finer-grained alluvial materials such as muddy floodplain deposits were removed.

The erosion process that picked-out these features in inverted relief was presumably wind-action, active over several billions years of martian history. However, the main fan body also shows evidence for late-stage fluvial erosion: a ∼1 km wide channel incises the upper surface (Fig. 3a). This suggests later fluvial flow to a lower base level (< −2750) than was present during the formation of the main fan body (∼ −2450 to ∼ −2650) which it cuts though.

3.8. Timing of sedimentation of the Hypanis sediment fan

The western and southern branches of Hypanis Valles originate within the continuous ejecta blanket of a ∼70 km diameter unnamed crater in the Hypanis catchment (Fig. 2). The southern branch parallels the distal reach of Nanedi Valles and has a relatively low width of ∼300 m. The western branch emerges with a width of ∼1.2 km. Both channels show clear structures and topographic expression except where they are superposed by the ejecta of the unnamed crater, which mutes the structure and topography of the channels. These observations, coupled with the superposition of secondary crater chains from the same unnamed crater, indicate that Hypanis Valles pre-dates the formation of this crater. CTX-derived impact crater statistics taken from the crater's continuous ejecta blanket indicate a N(1) value of 4630 craters per 10^6 km^2. This equates to an early Hesperian age using both Hartmann (2005) and Ivanov et al. (2001) production functions and the Michael (2013) and Hartmann and Neukum (2001) chronology functions (Fig. 8). Buffered crater counts on Hypanis Valles, using both the 1 radii and 3 radii methods, indicate a similar early Hesperian age based on the N(1) value using the Ivanov et al. (2001) and Hartmann and Neukum (2001) production and chronology functions. Using the Hartmann (2005), and Michael (2013) functions, the N(1) value suggests a late Noachian age. Both the superposition relationships between the unnamed crater and Hypanis Valles and the chronology data are generally consistent with previous age constraints (Fassett and Head, 2008) that placed Hy-

panis within the latest stage of the early climate optimum of valley network formation, at ~3.6 Ga, in the early Hesperian (Irwin et al., 2005).

4. Toward a deltaic interpretation for the Hypanis fan system

It remains difficult to distinguish fluvial fan deposits on Mars from deltaic bodies from orbital morphological analyses alone. Preserved fan remnants on Mars are not exact mimics of delta geomorphology as the stratigraphy represents the time integrated evolution of deltaic processes. The absence of well exposed exhumed planforms of ancient fluvial deltas on Earth limits comparison to martian examples, unlike with fluvial systems. Here, we posit on the basis of palaeogeomorphic observations that the Hypanis sediment fan represents an ancient martian delta deposited at the margin of a standing waterbody in the Chryse basin. In its proximal region, the Hypanis fan forms a radially symmetric palaeogeomorphic feature in planform that developed immediately downstream of the Hypanis Valles bedrock channel outlet. Deposition of the fan at this location is likely the consequence of the transition from confinement of flow in the upland bedrock channel to a basin where flow is unconfined (e.g., Blair and McPherson, 1994; Sittoni et al., 2014). Here, reduction in channel bed and water surface slopes reduced the sediment transport capacity leading to enhanced deposition proximal to the valley outlet. In detail, the radially symmetric planform deposit of the proximal Hypanis fan appears to comprise an amalgamation of several lobe-like remnants of formerly more extensive deposits. One interpretation of the proximal fan is that it was formed by avulsion of river channels around the topographically pinned node of the Hypanis outlet, which created multiple, laterally stacked deposits. In this case, the outlet forms a bedslope-mediated avulsion node (Ganti et al., 2014).

For the proximal fan, it is unclear whether it represents a purely fluvial fan or a deltaic body. We note however that the stratigraphy preserved on the proximal fan exhumed surface comprises relatively straight to slightly curved lineations that radiate outward from the Hypanis outlet. We interpret the lineations as preserved bedset boundaries and/or channel margins exposed on the planform surface. No evidence for sinuous channels characterised by lateral accretion bedding, as recorded in both the Jezero and Eberswalde systems, is observed (Bhattacharya et al., 2005; Goudge et al., 2015). The presence of lineations showing a large spread in azimuth emanating from the bedrock outlet is suggestive of deposition by multiple channel bodies that have become laterally stacked and further suggests frequent avulsive shifting of channels downstream of the outlet. Discrete ribbon channels are not observed. This is similar to channel-fill deposits described by Goudge et al. (2017) from the uppermost preserved surface of the Jezero delta, which they interpret as deposition from a highly avulsive fluvial system near or within the backwater zone of a delta. Such a model may also apply to the proximal Hypanis deposits. Moreover, we note evidence in the proximal fan for divergence of lineations, and hence channel orientation, within the fan body itself which we interpret to represent channel bifurcations in downstream locations on the fan and not just at the outlet comparable to distributary features observed in terrestrial deltas (Chamberlain et al., 2018). Such fan-top furcations are typical of distributary channels in delta top environments. In this case, avulsion nodes occur in the backwater zone, a region characterised by high water surface slope variability and which shows spatial flow deceleration and deposition at low flows termed 'backwater-mediated' avulsions (Chatanantavet et al., 2012; Chatanantavet and Lamb, 2014; Ganti et al., 2014). The proximal Hypanis fan deposits show bifurcation of channels downstream of the outlet, however the preservation of distinct patterns with high bifurcation angles is limited.

The most-clear evidence for a deltaic origin for the Hypanis system comes from the morphology of Channel-Lobe system X (Fig. 5). Here, formation of an arcuate lobe-shaped deposit occurs ~50 km downstream of the Hypanis outlet, overstepping beyond the depositional edge of the proximal fan. We propose that the lobe-shaped deposit formed at the mouth of the channel due to polyfurcation of distributaries from the main channel. Within the lobe individual channels cannot be observed though lineations are observed diverging from the channel on the upper surface of the lobe. We posit that the channel-lobe transition represents a furcation point of the delta distributary network and records a palaeoshoreline position (Chamberlain et al., 2018). Amplitude stratal slices through 3D seismic data across deltaic successions show similar development of deltaic lobes developed at the ends of distributaries as deltaic systems prograded basinwards (Zeng et al., 2013, 2012). The location of the channel-lobe transition in system X north of the proximal fan indicates a major basinward jump in the location of the palaeoshoreline.

Whilst such a process of downstream migration in locus of deposition is possible in fluvial fans where feeder channels incise through proximal fan deposits, and new lobe deposition occurs downstream of the incised channel, at Hypanis we do not observe evidence that the feeder channel to Lobe X is incised into proximal deposits thus ruling out the above hypothesis. Instead, we suggest that the basinward-step of Lobe X is the consequence of downstream migration of a backwater-mediated avulsion site. In the case of Channel-lobe system X, the avulsion node has migrated basinward significantly compared to the proximal fan radius resulting in a highly elongated planform geometry (e.g., Fig. 4 in Ganti et al., 2014). We suggest that basinward migration of the zone of channel-lobe transition is the crucial evidence indicating that the Hypanis sediment fan represent a delta that prograded into a standing body of water. The fan complex was composed of multiple channels and lobes (Van Dijk et al., 2012, 2009), which formed at the margin of a large, standing body of water. Many of these channels and lobes have since been exhumed and are now preserved in inverted relief.

The sedimentary palaeogeomorphology at Hypanis indicates further significant basinward progradation of the sediment fan system. The inverted channel branches preserved at the eastern margin of the proximal fan (Fig. 6), demonstrate that fluvial sediment routing systems transported sediment up to at least 100 km northeast of the Hypanis outlet indicating significant expansion of the Hypanis sedimentary system north of the Chryse escarpment and the Xanthe Terra uplands. Here too, we observe an example of a major basinward jump in the position of the channel-lobe transition, as exemplified by Lobe Y (Fig. 7). It remains difficult to explain this channel-lobe transition in a purely fluvial fan setting.

An important observation is that the elevation of deposition of channel-lobe sediments of the Hypanis system occur at progressively lower elevations when traced basinward to the north. Deposits of the proximal fan occur at an elevation of ~−2500 m, whereas deposits of Lobe Y occur at ~−2700 m, and deposits further basinward are present at an elevation of ~−3000 m. The most parsimonious explanation for both the basinward migration of the avulsion node (the channel-lobe transition) and its downstepping in elevation is that the Hypanis fluvio-deltaic system records progradation of the sedimentary system during progressive fall in baselevel through a ~500 m elevation change, with the baselevel representing the elevation of a standing body of water. This assumes that the basin floor and upstream region are tectonically stable, which is likely valid for Mars up to the global scale (e.g.: Anderson et al., 2001; Citron et al., 2018). The scale of the Hypanis delta contrasts with the nearby Sabrina Valles fan system, which is smaller and has no obvious basinward-stepping fan remnants (Hauber et al., 2009).

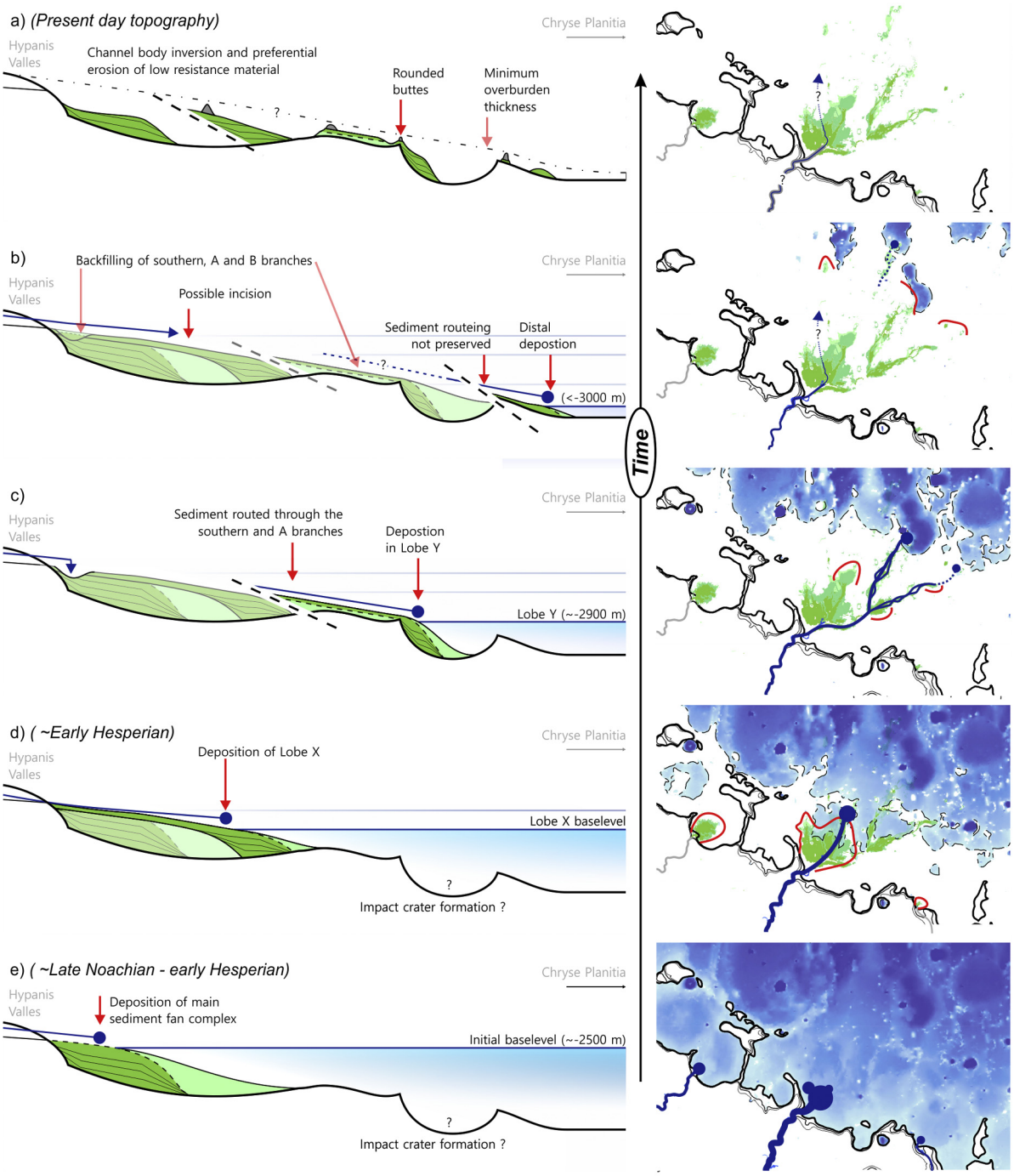

Fig. 9. The major stages in the development of the Hypanis Valles sediment fan system going backwards in time. The left shows an illustrative (S to N) cross-section with bright tones indicating the active processes and the right shows corresponding stages of plan view morphology in the contemporary outcrops. Resistant, coarser-grained material is indicated by dark green (lines indicate layering), less resistant finer-grained deposits are indicated by light green; the fluvial regime is a blue line and at the edge of a standing body of water is shown in blue. Also shown are the rounded buttes, which are remnants of a regional, low resistance overburden.

From the above considerations, we construct the following scenario as a possible sequence of events in the depositional history of Hypanis Valles (Fig. 9).

1. Deposition of the arcuate proximal fan at a base level of ~ -2500 m about the bedrock-confined outlet of Hypanis Valles. The fan body comprises a complex assemblage of laterally merged lobes and feeder channels with an area of >970 km^2.
2. Progradation of Channel-Lobe system X. During the first stage of base level fall, the locus of deposition shifted basinwards and Lobe X stepped out from the proximal fan.
3. Extension of fluvial systems north- and northeast-wards at the eastern margin of the proximal up to ~100 km basinwards of the Hypanis outlet.
4. Deposition of Lobe Y at the termination of Inverted Channel Branch A. Continued advance of the depositional locus due to base level fall to ~ -2700 m.

5. Further basinward extension of the sediment routing system and deposition of distal fan elements at a base level of ∼−3000 m.
6. Denudation and channel body inversion. Aeolian erosion deflated the land surface, preferentially removing less-resistant materials the remaining outcrops of which are likely to be the isolated rounded buttes and crucially creating the inverted channel bodies (Figs. 4, 6, 7 and supplementary material).

5. Wider implications

The palaeomorphology and stratigraphic architecture of the Hypanis fan complex are consistent with initial delta deposits forming at an elevation of ∼−2500 m. The system then prograded by at least 140 km basinwards in response to a base level fall to an elevation of ∼−3000 m. This fall in baselevel represents more than half a vertical kilometre of water-level change. This relative change is more important than the absolute elevations because of the possible influence of global scale crustal flexure, Citron et al. (2018) report that the area of the Hypanis sediment fan may have been displaced by −1000 m due to true polar wander and the development of Tharsis. The identification of delta deposits here provides evidence for a large standing body of water that likely began to retreat at the start of the Hesperian. Importantly, the basin at the outlet of Hypanis Valles is open downslope to Chryse Planitia, which in turn opens downslope onto the northern plains. The interpretation of the Hypanis sediment fan as a prograding delta system is therefore also evidence for the existence and demise of a regional body of water which extended across Chryse Planitia, and potentially even a larger-scale water body – an ocean – that might have extended across the northern plains of Mars during the early Hesperian (Fig. 8).

The maximum elevation (∼−2500 m) of the water body into which the main Hypanis sediment fan formed is similar to the elevation of the Sabrina Valles fan outlet (Fig. 2). It is also very similar to the elevation of morphological indicators of a possible northern ocean highstand, including (i) the proposed geomorphic "contact 1" and "Arabia shoreline" where the theoretical distribution of surface water during the Noachian is estimated to circumscribe the northern lowlands between −2550 m and −3380 m (Clifford and Parker, 2001), and (ii) the equipotential surface at −2540 m ± 117 (with a standard deviation of ∼120 m) of Di Achille and Hynek (2010) calculated from the elevation of 52 sediment fans observed on the margins of the northern lowlands (note: this study included the Hypanis fan). Unlike those previous investigations of possible ocean shorelines which identify geomorphic features across a wide area at a range of elevations, we specifically identify the range of elevations at a single location through which the level of the water body fell (−2500 m to ∼−3000 m) during a period when fluvial processes were still active. This provides a minimum range of elevations within which other ocean-related shoreline landforms could have existed along the highland-lowland dichotomy.

If correct, our interpretations have some significance for both the local and global martian palaeoclimate. Locally, within the catchment, the stratigraphic relations and crater size frequency distribution statistics from the upstream channel networks constrain activity of the drainage network and fan complex until the early Hesperian (Fig. 8). The ∼500 m drop in water level during the time recorded by the Hypanis deltaic deposits, however, may potentially reflect a decline in the abundance and stability of water globally at the martian surface after a late-Noachian global climate optimum (Irwin et al., 2005; Fassett and Head, 2008), though this requires further testing. Within this overall drying trend, fluvial flow within the catchment may have become increasingly ephemeral or episodic, as the availability of liquid water decreased. This transition is demonstrated in the older, high elevation parts of the Hypanis fan complex, which are incised by one or more late-stage erosional channels. Whilst poorly constrained, if the body of water the Hypanis delta system formed in was a northern ocean, that occupied the topography of the existing northern plains, we estimate a drop in water level of 500 m, from what is now −2500 m in elevation to −3000 m. Hence, the geology of the Hypanis fan deposits record environments from both Mars' climatic optimum, and from a period during which liquid water was beginning to play a decreasing role in modifying the martian landscape. In summary, the Hypanis fan sedimentary system offers an outstanding opportunity in a future robotic exploration mission to test the hypothesis of large seas or oceans in the northern plains of Mars from sedimentary records.

6. Conclusions

The Hypanis fan system consists of multiple, interconnected inverted channels and lobate fan-bodies, which extend out from the Hypanis Valles outlet and into the Chryse Planitia plains. From analysis of its palaeomorphology, we interpret the Hypanis fan system as an ancient delta deposit that formed at the margin of a standing body of water in the late Noachian or early Hesperian epochs. The extent of the delta deposits makes Hypanis the largest reported delta-fan system on Mars. Elements of the delta system extend at least 140 km northeast of the Hypanis Valles outlet, and descend 500 m in elevation. This downslope progradation of the delta deposits – or forced regression – is consistent with the retreat of a standing body of water across at least this horizontal and vertical extent. The fan deposits at Hypanis are not topographically confined, suggesting that the local basin was open to the much larger-scale Chryse Planitia topographic basin, and possibly a significant part of the northern plains of Mars. The sedimentary system therefore potentially records the late Noachian or early Hesperian highstand of a regional sea in Chryse Planitia, and potentially an even larger scale water body that formerly occupied parts of the northern lowlands. By the time that the most distal delta deposits at Hypanis had been emplaced, water levels had dropped by ∼500 m. This suggests that the delta formation at Hypanis spanned a time period during which Mars' climate underwent significant change.

Acknowledgements

The authors would like to thank Vic Baker and an anonymous reviewer for their timely and thorough reviews. We gratefully acknowledge the support of the UK Space Agency and the UK Science and Technology Facilities Council (STFC) for supporting science relating to ExoMars Rover landing site selection activities and Trace Gas Orbiter participating scientists via the following grants: ST/L006456/1 and ST/L00254X/1 (PMG), ST/K502388/1 and ST/R002355/1 (JMD), ST/L00643X/1 (PF, MRB, SG, ES-N), ST/R001413/1 (PF, MRB, PG) and ST/L006413/1 (SG). NW was partially funded by NASA Mars Data Analysis grant NNX14AL09G.

Appendix A. Supplementary material

Supplementary material related to this article can be found online at https://doi.org/10.1016/j.epsl.2018.07.040.

References

Adler, J.B., Bell, J.F., Fawdon, P., Davis, J., Warner, N.H., Sefton-Nash, E., Harrison, T.N., 2018. Hypotheses for the origin of the Hypanis fan-shaped deposit at the edge of the Chryse escarpment, Mars: is it a delta? Icarus. https://doi.org/10.1016/j.icarus.2018.05.021.

Anderson, R.C., Dohm, J.M., Golombek, M.P., Haldemann, A.F.C., Franklin, B.J., Tanaka, K.L., Lias, J., Peer, B., 2001. Primary centers and secondary concentrations of tectonic activity through time in the western hemisphere of Mars. J. Geophys. Res., E Planets 106, 20563–20585.

Ansan, V., Loizeau, D., Mangold, N., Le Mouélic, S., Carter, J., Poulet, F., Dromart, G., Lucas, A., Bibring, J.-P., Gendrin, A., Gondet, B., Langevin, Y., Masson, P., Murchie, S., Mustard, J.F., Neukum, G., 2011. Stratigraphy, mineralogy, and origin of layered deposits inside Terby crater, Mars. Icarus 211, 273–304. https://doi.org/10.1016/j.icarus.2010.09.011.

Balme, M., Berman, D.C., Bourke, M.C., Zimbelman, J.R., 2008. Transverse Aeolian Ridges (TARs) on Mars. Geomorphology 101, 703–720. https://doi.org/10.1016/j.geomorph.2008.03.011.

Barker, Donald C., Bhattacharya, Janok P., 2018. Sequence stratigraphy on an early wet Mars. Planet. Space Sci. 151, 97–108.

Barlow, N.G., Boyce, J.M., Costard, F.M., Craddock, R.A., Garvin, J.B., Sakimoto, S.E.H., Kuzmin, R.O., Roddy, D.J., Soderblom, L.A., 2000. Standardizing the nomenclature of Martian impact crater ejecta morphologies. J. Geophys. Res. 105, 26733–26738. https://doi.org/10.1029/2000je001258.

Bhattacharya, J.P., Payenberg, T.H.D., Lang, S.C., Bourke, M., 2005. Dynamic river channels suggest a long-lived Noachian crater lake on Mars. Geophys. Res. Lett. 32. https://doi.org/10.1029/2005GL022747.

Blair, T.C., McPherson, J.G., 1994. Alluvial fans and their natural distinction from rivers based on morphology, hydraulic processes, sedimentary processes, and facies assemblages. J. Sediment. Res. 64 (3a), 450–489.

Boynton, W.V., Feldman, W.C., Squyres, S.W., Prettyman, T.H., Brückner, J., Evans, L.G., Reedy, R.C., Starr, R., Arnold, J.R., Drake, D.M., Englert, P.A.J., Metzger, A.E., Mitrofanov, I., Trombka, J.I., d'Uston, C., Wänke, H., Gasnault, O., Hamara, D.K., Janes, D.M., Marcialis, R.L., Maurice, S., Mikheeva, I., Taylor, G.J., Tokar, R., Shinohara, C., 2002. Distribution of hydrogen in the near surface of Mars: evidence for subsurface ice deposits. Science 297, 81–85.

Burr, D.M., Bruno, B.C., Lanagan, P.D., Glaze, L.S., Jaeger, W.L., Soare, R.J., Wan Bun Tseung, J.-M., Skinner Jr., J.A., Baloga, S.M., 2009. Mesoscale raised rim depressions (MRRDs) on Earth: a review of the characteristics, processes, and spatial distributions of analogs for Mars. Planet. Space Sci. 57, 579–596. https://doi.org/10.1016/j.pss.2008.11.011.

Cardenas, B.T., Mohrig, D., Goudge, T.A., 2018. Fluvial stratigraphy of valley fills at Aeolis Dorsa, Mars: evidence for base-level fluctuations controlled by a downstream water body. GSA Bull. 130 (3–4), 484–498.

Carr, M.H., Head, J.W., 2015. Martian surface/near-surface water inventory: sources, sinks, and changes with time. Geophys. Res. Lett. 42, 2014GL062464. https://doi.org/10.1002/2014GL062464.

Carr, M.H., Head, J.W., 2003. Oceans on Mars: an assessment of the observational evidence and possible fate. J. Geophys. Res., Planets 108. https://doi.org/10.1029/2002JE001963.

Chamberlain, E.L., Törnqvist, T.E., Shen, Z., Mauz, B., Wallinga, J., 2018. Anatomy of Mississippi Delta growth and its implications for coastal restoration. Sci. Adv. 4. https://doi.org/10.1126/sciadv.aar4740.

Chatanantavet, Phairot, Lamb, Michael P., 2014. Sediment transport and topographic evolution of a coupled river and river plume system: an experimental and numerical study. J. Geophys. Res., Earth Surf. 119, 1263–1282. https://doi.org/10.1002/2013JF002810.

Chatanantavet, Phairot, Lamb, Michael P., Nittrouer, Jeffrey A., 2012. Backwater controls of avulsion location on deltas. Geophys. Res. Lett. 39. https://doi.org/10.1029/2011GL050197.

Christensen, P., Jakosky, B., Kieffer, H., Malin, M., McSween, H., Nealson, K., Mehall, G., Silverman, S., Ferry, S., Caplinger, M., Ravine, M., 2004. The Thermal Emission Imaging System (THEMIS) for the Mars 2001 Odyssey mission. Space Sci. Rev. 110, 85–130. https://doi.org/10.1023/b:spac.0000021008.16305.94.

Citron, R.I., Manga, M., Hemingway, D.J., 2018. Timing of oceans on Mars from shoreline deformation. Nature 555, 643.

Clifford, S.M., Parker, T.J., 2001. The evolution of the Martian hydrosphere: implications for the fate of a primordial ocean and the current state of the northern plains. Icarus 154, 40–79. https://doi.org/10.1006/icar.2001.6671.

Costard, F., Séjourné, A., Kelfoun, K., Clifford, S., Lavigne, F., Di Pietro, I., Bouley, S., 2017. Modeling tsunami propagation and the emplacement of thumbprint terrain in an early Mars ocean. J. Geophys. Res., Planets 122, 633–649. https://doi.org/10.1002/2016JE005230.

Craddock, R.A., Maxwell, T.A., Howard, A.D., 1997. Crater morphometry and modification in the Sinus Sabaeus and Margaritifer Sinus regions of Mars. J. Geophys. Res., Planets 102, 13321–13340. https://doi.org/10.1029/97JE01084.

Cuevas Martínez, J.L., Cabrera Pérez, L., Marcuello, A., Arbués Cazo, P., Marzo Carpio, M., Bellmunt, F., 2010. Exhumed channel sandstone networks within fluvial fan deposits from the Oligo-Miocene Caspe Formation, South-east Ebro Basin (North-east Spain). Sedimentology 57 (1), 162–189. https://doi.org/10.1111/j.1365-3091.2009.01096.x.

Davis, J.M., Balme, M., Grindrod, P.M., Williams, R.M.E., Gupta, S., 2016. Extensive Noachian fluvial systems in Arabia Terra: implications for early Martian climate. Geology 44 (10), 847–850.

Di Achille, G., Hynek, B.M., 2010. Ancient ocean on Mars supported by global distribution of deltas and valleys. Nat. Geosci. 3, 459–463.

DiBiase, R.A., Limaye, A.B., Scheingross, J.S., Fischer, W.W., Lamb, M.P., 2013. Deltaic deposits at Aeolis Dorsa: sedimentary evidence for a standing body of water on the northern plains of Mars. J. Geophys. Res., Planets 118, 1285–1302. https://doi.org/10.1002/jgre.20100.

Esri, 2016. How watershed works. Watershed Works.

Fassett, C.I., Head, J.W., 2008. The timing of martian valley network activity: constraints from buffered crater counting. Icarus 195, 61–89. https://doi.org/10.1016/j.icarus.2007.12.009.

Ganti, V., Chu, Z., Lamb, M.P., Nittrouer, J.A., Parker, G., 2014. Testing morphodynamic controls on the location and frequency of river avulsions on fans versus deltas: Huanghe (Yellow River), China. Geophys. Res. Lett. 41, 7882–7890. https://doi.org/10.1002/2014GL061918.

Gibling, M., Rust, B., 1990. Ribbon sandstones in the Pennsylvanian Waddens Cove formation, Sydney Basin, Atlantic Canada: the influence of siliceous duricrusts on channel-body geometry. Sedimentology 37, 45–66. https://doi.org/10.1111/j.1365-3091.1990.tb01982.x.

Goudge, T.A., Milliken, R.E., Head, J.W., Mustard, J.F., Fassett, C.I., 2017. Sedimentological evidence for a deltaic origin of the western fan deposit in Jezero crater, Mars and implications for future exploration. Earth Planet. Sci. Lett. 458, 357–365. https://doi.org/10.1016/j.epsl.2016.10.056.

Goudge, T.A., Mustard, J.F., Head, J.W., Fassett, C.I., Wiseman, S.M., 2015. Assessing the mineralogy of the watershed and fan deposits of the Jezero crater paleolake system, Mars. J. Geophys. Res., Planets 120, 775–808. https://doi.org/10.1002/2014JE004782.

Grotzinger, J.P., Gupta, S., Malin, M.C., Rubin, D.M., Schieber, J., Siebach, K., Sumner, D.Y., et al., 2015. Deposition, exhumation, and paleoclimate of an ancient lake deposit, Gale crater, Mars. Science 350 (6257), aac7575.

Gupta, S., 1997. Himalayan drainage patterns and the origin of fluvial megafans in the Ganges foreland basin. Geology 25, 11–14. https://doi.org/10.1130/0091-7613(1997)025<0011:HDPATO>2.3.CO;2.

Hartmann, W.K., 2005. Martian cratering 8: isochron refinement and the chronology of Mars. Icarus 174, 294–320.

Hartmann, W.K., Neukum, G., 2001. Cratering chronology and the evolution of Mars. Space Sci. Rev. 96, 165–194. https://doi.org/10.1023/a:1011945222010.

Hauber, E., Gwinner, K., Kleinhans, M., Reiss, D., Di Achille, G., Ori, G.-G., Scholten, F., Marinangeli, L., Jaumann, R., Neukum, G., 2009. Sedimentary deposits in Xanthe Terra: implications for the ancient climate on Mars. In: Eur. Mars Sci. Explor. Conf. EMSEC. Planet Space Sci. 57, 944–957. https://doi.org/10.1016/j.pss.2008.06.009.

Hauber, E., Platz, T., Reiss, D., Le Deit, L., Kleinhans, M.G., Marra, W.A., de Haas, T., Carbonneau, P., 2013. Asynchronous formation of Hesperian and Amazonian-aged deltas on Mars and implications for climate. J. Geophys. Res., Planets 118, 1529–1544. https://doi.org/10.1002/jgre.20107.

Hynek, B.M., Beach, M., Hoke, M.R.T., 2010. Updated global map of Martian valley networks and implications for climate and hydrologic processes. J. Geophys. Res., Planets 115. https://doi.org/10.1029/2009JE003548.

Irwin, I., Rossman, P., Craddock, R.A., Howard, A.D., 2005. Interior channels in Martian valley networks: discharge and runoff production. Geology 33, 489–492. https://doi.org/10.1130/G21333.1.

Irwin, R.P., Lewis, K.W., Howard, A.D., Grant, J.A., 2015. Paleohydrology of Eberswalde crater, Mars. In: Planet. Geomorphol. Proc. 45th Annu. Binghamt. Geomorphol. Symp. Held 12–14 Sept. 2014, Knoxv., Tenn., USA. Geomorphology 240, 83–101. https://doi.org/10.1016/j.geomorph.2014.10.012.

Irwin, R.P., Tanaka, K.L., Robbins, S.J., 2013. Distribution of Early, Middle, and Late Noachian cratered surfaces in the Martian highlands: implications for resurfacing events and processes. J. Geophys. Res., Planets 118, 278–291. https://doi.org/10.1002/jgre.20053.

Ivanov, B., Neukum, G., Wagner, R., 2001. Size-frequency distributions of planetary impact craters and asteroids. In: Collisional Processes in the Solar System. Springer, pp. 1–34.

Kirk, R.L., Howington-Kraus, E., Rosiek, M.R., Anderson, J.A., Archinal, B.A., Becker, K.J., Cook, D.A., Galuszka, D.M., Geissler, P.E., Hare, T.M., Holmberg, I.M., Keszthelyi, L.P., Redding, B.L., Delamere, W.A., Gallagher, D., Chapel, J.D., Eliason, E.M., King, R., McEwen, A.S., 2008. Ultrahigh resolution topographic mapping of Mars with MRO HiRISE stereo images: meter-scale slopes of candidate Phoenix landing sites. J. Geophys. Res., Planets 113, E00A24. https://doi.org/10.1029/2007JE003000.

Knade, J., Hauber, E., Platz, T., Le Deit, L., Kinch, K., 2017. Detailed geological mapping of the fluvial deposits in Magong crater, Xanthe Terra, Mars. In: European Planetary Science Congress, vol. 11.

Kneissl, T., Michael, G.G., Platz, T., Walter, S.H.G., 2015. Age determination of linear surface features using the Buffered Crater Counting approach – case studies of the Sirenum and Fortuna Fossae graben systems on Mars. Icarus 250, 384–394. https://doi.org/10.1016/j.icarus.2014.12.008.

Kraal, E.R., van Dijk, M., Postma, G., Kleinhans, M.G., 2008. Martian stepped-delta formation by rapid water release. Nature 451, 973–976. https://doi.org/10.1038/nature06615.

Malin, M.C., Bell III, J.F., Cantor, B.A., Caplinger, M.A., Calvin, W.M., Clancy, R.T., Edgett, K.S., Edwards, L., Haberle, R.M., James, P.B., Lee, S.W., Ravine, M.A., Thomas, P.C., Wolff, M.J., 2007. Context camera investigation on board the Mars

reconnaissance orbiter. J. Geophys. Res. 112, E05S04. https://doi.org/10.1029/2006je002808.

McEwen, A.S., Eliason, E.M., Bergstrom, J.W., Bridges, N.T., Hansen, C.J., Delamere, W.A., Grant, J.A., Gulick, V.C., Herkenhoff, K.E., Keszthelyi, L., Kirk, R.L., Mellon, M.T., Squyres, S.W., Thomas, N., Weitz, C.M., 2007. Mars reconnaissance orbiter's high resolution imaging science experiment (HiRISE). J. Geophys. Res. 112, E05S02. https://doi.org/10.1029/2005je002605.

Michael, G.G., 2013. Planetary surface dating from crater size–frequency distribution measurements: multiple resurfacing episodes and differential isochron fitting. Icarus 226, 885–890. https://doi.org/10.1016/j.icarus.2013.07.004.

Moore, J.M., Howard, A.D., Dietrich, W.E., Schenk, P.M., 2003. Martian layered fluvial deposits: implications for Noachian climate scenarios. Geophys. Res. Lett. 30. https://doi.org/10.1029/2003GL019002.

Nelson, D.M., Greeley, R., 1999. Geology of Xanthe Terra outflow channels and the Mars Pathfinder landing site. J. Geophys. Res., Planets 104, 8653–8669. https://doi.org/10.1029/98JE01900.

Pain, C.F., Clarke, J.D.A., Thomas, M., 2007. Inversion of relief on Mars. In: Deep Impact Mission Comet 9PTempel 1, Part 2. Icarus 190 (2), 478–491. https://doi.org/10.1016/j.icarus.2007.03.017.

Pain, C.F., Oilier, C.D., 1995. Inversion of relief – a component of landscape evolution. Geomorphology 12, 151–165. https://doi.org/10.1016/0169-555X(94)00084-5.

Parker, et al., 1993. Coastal geomorphology of the Martian northern plains. J. Geophys. Res., Planets 98 (E6), 11061–11078. https://doi.org/10.1029/93JE00618.

Platz, T., Hauber, E., Le Deit, L., Van Gasselt, S., Kinch, K., Madsen, M.B., Rosenberg, H., 2014. Landing at the terminus of Sabrina Vallis: a potential 2020 Mars rover landing site. In: European Planetary Science Congress, vol. 9.

Ramirez, R.M., Craddock, R.A., 2018. The geological and climatological case for a warmer and wetter early Mars. Nat. Geosci. 11, 230–237. https://doi.org/10.1038/s41561-018-0093-9.

Rice, M., Belll III, J., Gupta, S., Warner, N., Goddard, K., Anderson, R., 2013. A detailed geologic characterization of Eberswalde crater, Mars. Int. J. Mars Sci. Explor. 8, 15–57.

Rodriguez, J.A.P., Fairén, A.G., Tanaka, K.L., Zarroca, M., Linares, R., Platz, T., Komatsu, G., Miyamoto, H., Kargel, J.S., Yan, J., Gulick, V., Higuchi, K., Baker, V.R., Glines, N., 2016. Tsunami waves extensively resurfaced the shorelines of an early Martian ocean. Sci. Rep. 6, 25106.

Salvatore, M.R., Christensen, P.R., 2014. On the origin of the Vastitas Borealis Formation in Chryse and Acidalia Planitiae, Mars. J. Geophys. Res., Planets 119, 2437–2456. https://doi.org/10.1002/2014JE004682.

Schon, S.C., Head, J.W., Fassett, C.I., 2012. An overfilled lacustrine system and progradational delta in Jezero crater, Mars: implications for Noachian climate. Planet. Space Sci. 67, 28–45. https://doi.org/10.1016/j.pss.2012.02.003.

Sefton-Nash, E., Fawdon, P., Gupta, S., Balme, M., Davis, J., Grindrod, P., Sidiropoulos, P., Yershov, V., Muller, J.-P., 2015. The Hypanis Fluvial Deltaic System in Xanthe Terra: A Candidate ExoMars 2018 Rover Landing Site.

Sittoni, L., Paola, C., Voller, V., 2014. Geometry, flow, and sediment transport of alluvial deposits induced by topographically driven flow expansions. J. Sediment. Res. 84, 122–135. https://doi.org/10.2110/jsr.2014.11.

Smith, D.E., Zuber, M.T., Frey, H.V., Garvin, J.B., Head, J.W., Muhleman, D.O., Pettengill, G.H., Phillips, R.J., Solomon, S.C., Zwally, H.J., Banerdt, W.B., Duxbury, T.C., Golombek, M.P., Lemoine, F.G., Neumann, G.A., Rowlands, D.D., Aharonson, O., Ford, P.G., Ivanov, A.B., Johnson, C.L., McGovern, P.J., Abshire, J.B., Afzal, R.S., Sun, X., 2001. Mars Orbiter Laser Altimeter: experiment summary after the first year of global mapping of Mars. J. Geophys. Res. 106, 23689–23722. https://doi.org/10.1029/2000je001364.

Strahler, A.N., 1957. Quantitative analysis of watershed geomorphology. Eos 38, 913–920. https://doi.org/10.1029/TR038i006p00913.

Tanaka, K.L., Skinner, J.A., Dohm, J., Irwin III, R.P., Kolb, E.J., Fortezzo, C.M., Platz, T., Michael, G.G., Hare, T.M., 2014. Geologic map of Mars: U.S. Geological Survey Scientific Investigations Map 3292, scale 1:20,000,000, pamphlet 43 p.

Van Dijk, M., Kleinhans, M.G., Postma, G., Kraal, E., 2012. Contrasting morphodynamics in alluvial fans and fan deltas: effect of the downstream boundary. Sedimentology 59, 2125–2145.

Van Dijk, M., Postma, G., Kleinhans, M.G., 2009. Autocyclic behaviour of fan deltas: an analogue experimental study. Sedimentology 56, 1569–1589.

Villanueva, G.L., Mumma, M.J., Novak, R.E., Käufl, H.U., Hartogh, P., Encrenaz, T., Tokunaga, A., Khayat, A., Smith, M.D., 2015. Strong water isotopic anomalies in the martian atmosphere: probing current and ancient reservoirs. Science 348, 218. https://doi.org/10.1126/science.aaa3630.

Warner, N.H., Gupta, S., Calef, F., Grindrod, P., Boll, N., Goddard, K., 2015. Minimum effective area for high resolution crater counting of martian terrains. Icarus 245, 198–240.

Williams, R.M.E., Irwin III, R.P., Zimbelman, J.R., 2009. Evaluation of paleohydrologic models for terrestrial inverted channels: implications for application to martian sinuous ridges. Geomorphology 107, 300–315. https://doi.org/10.1016/j.geomorph.2008.12.015.

Wilson, S., Howard, A., Moore, J., Grant, J., 2007. Geomorphic and stratigraphic analysis of Crater Terby and layered deposits north of Hellas basin, Mars. J. Geophys. Res., Planets 112. https://doi.org/10.1029/2006JE002830.

Wordsworth, R.D., Kerber, L., Pierrehumbert, R.T., Forget, F., Head, J.W., 2015. Comparison of "warm and wet" and "cold and icy" scenarios for early Mars in a 3-D climate model: warm and wet vs. cold and icy early Mars. J. Geophys. Res., Planets 120, 1201–1219. https://doi.org/10.1002/2015JE004787.

Zaki, A.S., Pain, C.F., Edgett, K.S., Giegengack, R., 2018. Inverted stream channels in the Western Desert of Egypt: synergistic remote, field observations and laboratory analysis on Earth with applications to Mars. Icarus 309, 105–124. https://doi.org/10.1016/j.icarus.2018.03.001.

Zeng, H., Zhu, X., Zhu, R., 2013. New insights into seismic stratigraphy of shallow-water progradational sequences: subseismic clinoforms. Interpret. 1, SA35–SA51. https://doi.org/10.1190/INT-2013-0017.1.

Zeng, H., Zhu, X., Zhu, R., Zhang, Q., 2012. Guidelines for seismic sedimentologic study in non-marine postrift basins. Pet. Explor. Dev. 39, 295–304. https://doi.org/10.1016/S1876-3804(12)60045-7.